Faculdade de Engenharia da Universidade do Porto

Departamento de Engenharia Mecânica

# No-Load Torque Loss in a Planetary Gearbox

João Filipe

Master's Degree Dissertation presented to

Faculdade de Engenharia da Universidade do Porto

Dissertation supervised by

| | |
|---|---|
| Doctor Ramiro C. Martins | Researcher of INEGI |
| Professor Jorge H. O. Seabra | Full Professor of FEUP |
| Engineer Pedro M. T. Marques | Auxiliary Researcher of INEGI |

Porto, 2016

LaTeX

FEUP-U.PORTO

joão filipe

2016

*To my grandfather João Filipe,*
*with hope of honoring the name.*

# Acknowledgments

With the conclusion of the Master's Degree Thesis comes the time to mention some of the people who helped me throughout this final project.

I express my deepest appreciation to my supervisors, Dr. Jorge H. O. Seabra, Dr. Ramiro C. Martins and Eng. Pedro M. T. Marques, for the guidance during the execution of this work and for the inspiration that they represent as mechanical engineers. That's something I aspire for my future. I also show my recognition to Dr. José F. D. Rodrigues for encouraging me on the pursuit of excellence.

A special thanks to all of CETRIB (Unidade de Tribologia, Vibrações e Manutenção Industrial) researchers: Armando Campos, Beatriz Graça, José Brandão, Carlos Fernandes and David Gonçalves for providing me a good work environment and the availability at any moment. To my fellow Master's Degree colleagues I present my congratulations and offer a special acknowledgment for all the moments and advices.

At the end of the Master's Degree in Mechanical Engineering, a special reference to Faculdade de Engenharia da Universidade do Porto for these amazing years and resources put at the disposal of its students in order to provide them a superior education, professional and personally.

On a personal note, I express my gratitude to my girlfriend Ana Soares, for all the love and understanding and to all of my friends and colleagues with a special greeting to Álvaro Coutinho, who has been by my side since very young age and João Mota, who has been very important in this last six years.

Last, but no least, my family. The ones who gave me everything deserve the world. And that's my intention for my professional and personal future.

## Keywords

Power loss

No-load power loss

Planetary gears

Churning

Wind turbine gear oils

## Palavras-Chave

Perda de potência

Perda de potência em vazio

Engrenagens planetárias

Chapinagem

Lubrificantes para engrenagens de turbinas eólicas

# Abstract

Efficiency and environmental friendly are two expressions that go hand in hand with modern engineering. In every project the concern with these two aspects have acquired greater relevance over the years.

The growing degradation of the ozone layer shows the need for better usage of our resources. Renewable energy sources are taking a bigger role in our lives to fulfill that need. One of the most important is wind power, which relevance has been growing, namely in the European Union. Recently in Portugal, from May 7 to 11, the electricity consumption was fully covered by wind, solar and hydro power [1].

Wind turbines are capable of transforming the kinetic energy of the wind into mechanical energy, through a transmission system, which will power a electrical generator. The rotating speed of the turbine blades is quite low when compared with the input speed of the generator. In between the blades and the generator there is a multistage multiplier transmission. This transmission usually has 3 stages, being two of them planetary. Once as these turbines are able to transform power in the order of MW, a small efficiency increase must be considered.

In a planetary gearbox, load and no-load losses will occur. Studies have been made concerning the power loss of the gearbox components by Fernandes *et al.* [2]. Recently, Marques *et al.* [3] studied the overall efficiency of the planetary gearbox that is also being analyzed in this work.

The no-load losses, the main focus of this work, are dependent on the kinematics and geometry of the gearbox and also the lubricant properties. Several tests were performed under different conditions and four fully formulated wind turbine gear oils were selected.

One component of the no-load losses are the churning losses, result of viscous dissipation in the lubricant [4]. Despite the vast literature on the subject, studying this phenomenon presents a lot of challenges. None the less, a set of tests were performed in order to understand the dependence of this process on several factors.

# Resumo

Cada vez mais, em qualquer projeto de engenharia, a eficiência e a proteção ambiental são fatores a ter em consideração.

A degradação crescente da camada de ozono mostra a necessidade de um melhor aproveitamento dos recursos existentes à nossa disposição. Nesse sentido, as fontes de energia renovável estão a desempenhar um papel mais importante nas nossas vidas. A energia eólica é uma das mais importantes e com relevância crescente, nomeadamente na União Europeia. Recentemente em Portugal, de 7 a 11 de Maio, todo o consumo de eletricidade foi assegurado pelas energias renováveis, eólica, solar e hídrica [1].

As turbinas eólicas transformam a energia cinética do vento em energia mecânica, através de um sistema de transmissão, para ser aproveitada pelo gerador elétrico. Para tal acontecer é preciso ocorrer uma multiplicação para se atingirem as condições de funcionamento do gerador. Isto é conseguido com a utilização de vários andares, normalmente 3, sendo dois deles planetários. As turbinas são capazes de transformar potência na ordem do MW, pelo que qualquer pequeno aumento de eficiência deve ser considerado.

Numa caixa de engrenagens planetárias existem perdas em carga e perdas em vazio. Vários estudos foram levados a cabo para compreender estas perdas de potência. Fernandes *et al.* [2] analisaram a perda de potência nos componentes de uma caixa planetária e Marques *et al.* [3] verificaram a eficiência global desta . Este trabalho pretende dar continuidade a esses estudos.

As perdas em vazio, o foco principal desta tese, são dependentes não só da cinemática e geometria da caixa, mas também das propriedades do lubrificante e sistema de lubrificação. Vários testes foram realizados sob diferentes condições e com quatro óleos para engrenagens de turbinas eólicas.

Uma importante componente das perdas em vazio são as perdas de potência por chapinagem, resultado da dissipação viscosa no lubrificante [4]. Apesar de existirem vários artigos na literatura acerca deste assunto, o estudo deste fenómeno apresenta uma série de desafios. Ainda assim, foi realizado um conjunto de testes a fim de perceber como é que este processo varia com diversos fatores.

# Nomenclature

### Latin characters

| Variable | Description | Units |
|---|---|---|
| $A$ | Area of the immersed gear | $m^2$ |
| $a$ | Center distance | m |
| $a_i$ | Coefficient $i$ used for Ohlendorf model for the gear loss factor | - |
| $a_w$ | Working center distance | m |
| $B$ | Bearing width | m |
| $b$ | Gear face width | m |
| $b_i$ | Coefficient $i$ used for Xu Hai model for the coefficient of friction | - |
| $b_v$ | Constant that depends on the lubricant | °C |
| $C_1$ | Constant used for Höhn model | - |
| $C_2$ | Constant used for Höhn model | - |
| $C_M$ | Torque coefficient | - |
| $C_{Sp}$ | Constant used for Höhn model | - |
| $C_W$ | Variable used for the calculation of the drag frictional torque | - |
| $C_m$ | Dimensionless drag torque | - |
| $c$ | Constant that depends on the lubricant | °C |
| $D$ | Rolling bearing outside diameter | m |
| $D_a$ | Addendum diameter | m |
| $D_b$ | Base diameter | m |
| $D_p$ | Pitch diameter | m |
| $D_w$ | Working diameter | m |
| $d$ | Rolling bearing bore diameter | m |
| $d_S$ | Seal counterface diameter | m |
| $d_i$ | Immersion depth | m |
| $d_m$ | Bearing mean diameter | m |

| | | |
|---|---|---|
| $d_{sh}$ | Shaft diameter | m |
| $F_D$ | Factor that represents the influence of the temperature on the viscosity | - |
| $F_N$ | Normal force | N |
| $F_a$ | Axial force | N |
| $F_{bt}$ | Tooth normal force (transverse section) | N |
| $F_r$ | Radial force | N |
| $f_0$ | Coefficient that depends on bearing design and lubrication method | - |
| $f_1$ | Coefficient that depends on bearing design and lubrication method | - |
| $f_2$ | Coefficient that depends on bearing design and lubrication method | - |
| $f_A$ | Variable used for the calculation of the drag frictional torque | - |
| $Fr$ | Froude number | - |
| $G_{rr}$ | Variable used for the calculation of the rolling frictional torque | - |
| $G_{sl}$ | Variable used for the calculation of the sliding frictional torque | - |
| $g$ | Gravity acceleration | $m/s^2$ |
| $H$ | Oil level | m |
| $H_{Hohn}$ | Internal height of the gearbox | m |
| $H_V$ | Gear loss factor | - |
| $K$ | Constant that depends on the lubricant | $m^2/s$ |
| $K_L$ | Geometric constant | - |
| $K_{S1}$ | Geometric constant | - |
| $K_{S2}$ | Geometric constant | - |
| $K_{roll}$ | Variable used for the calculation of the drag frictional torque | - |
| $K_{rs}$ | Kinematic replenishment/starvation constant | - |
| $K_z$ | Geometric constant | - |
| $k_0$ | Variable used for Niemann model | - |
| $k \cdot m$ | Addendum coefficient | m |
| $L$ | Chord length of the immersed gear | m |
| $L_{Hohn}$ | Internal width of the gearbox | m |
| $l_1$ | Parameter used for Ohlendorf model | - |
| $l_D$ | Variable used for the calculation of the drag frictional torque | - |
| $l_H$ | Constant used for Höhn model | - |
| $M$ | Total frictional torque on a bearing | N·m |
| $M_C$ | Churning torque | N·m |

| | | |
|---|---|---|
| $M_{drag}$ | Drag frictional torque | N·m |
| $M_{load}$ | Load torque | N·m |
| $M_{rr}$ | Rolling frictional torque | N·m |
| $M_{seal}$ | Frictional torque of seals | N·m |
| $M_{sl}$ | Sliding torque | N·m |
| $m$ | Module | m |
| $m_1$ | Parameter used for Ohlendorf model | - |
| $n$ | Rotation speed | rad/s |
| $n_1$ | Parameter used for Ohlendorf model | - |
| $P_1$ | Equivalent bearing load | N |
| $P_{IN}$ | Input power | W |
| $P_V$ | Gearbox power loss | W |
| $P_{VD}$ | Seals power loss | W |
| $P_{VL}$ | Bearings power loss | W |
| $P_{VL0}$ | Bearings no-load power loss | W |
| $P_{VX}$ | Auxiliary power loss | W |
| $P_{VZ0}$ | Gears no-load power loss | W |
| $P_{VZP}$ | Gears load power loss | W |
| $P_h$ | Maximum Hertzian pressure | $N/m^2$ |
| $p_h$ | Contact pressure | $N/m^2$ |
| $p_r$ | Reference value of contact pressure | $N/m^2$ |
| $R$ | Radius of curvature | - |
| $R_1$ | Geometric constant | - |
| $R_2$ | Geometric constant | - |
| $R_S$ | Variable used for the calculation of the drag frictional torque | - |
| $R_a$ | Outside radius | m |
| $R_p$ | Pitch radius | m |
| $Ra$ | Average roughness | m |
| $Re$ | Reynolds number | - |
| $Rec$ | Critical Reynolds number | - |
| $S$ | Surface roughness | m |
| $S_1$ | Geometric constant | - |
| $S_2$ | Geometric constant | - |
| $S1$ | Counterclockwise rotation | - |

| | | |
|---|---|---|
| $S2$ | Clockwise rotation | - |
| $SR$ | Slide-to-roll ratio | - |
| $T_{VL}$ | Total frictional torque on a bearing | N·m |
| $T_{VL0}$ | No-load frictional torque on a bearing | N·m |
| $T_{VLP1}$ | Load frictional torque on a bearing | N·m |
| $T_{VLP2}$ | Load frictional torque on a bearing | N·m |
| $t$ | Variable used for the calculation of the drag frictional torque | - |
| $u$ | Gear ratio | - |
| $V_1$ | Volume of the immersed gear | $m^3$ |
| $V_M$ | Drag loss factor | - |
| $V_{R,EHL}$ | Reference value of speed for fluid friction | m/s |
| $V_{R,F}$ | Reference value of speed for boundary friction | m/s |
| $V_e$ | Entraining speed | m/s |
| $V_m$ | Volume of the oil bath | $m^3$ |
| $V_\epsilon$ | Total immersed volume | $m^3$ |
| $V_\Sigma$ | Sum speed | m/s |
| $v_g$ | Sliding speed | m/s |
| $v_t$ | Pitch line speed | m/s |
| $v_{\Sigma C}$ | Sum speed at pitch point | m/s |
| $X_L$ | Lubricant parameter | - |
| $X_R$ | Variable used for Michaelis model | - |
| $x$ | Profile shift coefficient | - |
| $Y$ | Axial load factor for single row bearings | - |
| $z$ | Number of teeth of a gear | - |

### Greek characters

| **Variable** | **Description** | **Units** |
|---|---|---|
| $\alpha$ | Pressure angle | rad |
| $\alpha_{EHL}$ | Parameter derived from experimental data | - |
| $\alpha_F$ | Parameter derived from experimental data | - |
| $\alpha_k$ | Thermal expansion coefficient | $K^{-1}$ |
| $\alpha_p$ | Piezoviscosity | $Pa^{-1}$ |
| $\alpha_t$ | Transverse pressure angle | rad |
| $\alpha_{tw}$ | Working transverse pressure angle | rad |

| | | |
|---|---|---|
| $\beta$ | Helix angle | rad |
| $\beta_1$ | Geometric constant | - |
| $\beta_F$ | Parameter derived from experimental data | - |
| $\beta_b$ | Base helix angle | rad |
| $\beta_t$ | Thermoviscosity | $K^{-1}$ |
| $\gamma$ | Acceleration | $m/s^2$ |
| $\gamma_{EHL}$ | Parameter derived from experimental data | - |
| $\epsilon_1$ | Addendum contact ratio of the driving gear | - |
| $\epsilon_2$ | Addendum contact ratio of the driven gear | - |
| $\epsilon_\alpha$ | Transverse contact ratio | - |
| $\eta$ | Dynamic viscosity | Pa·s |
| $\theta$ | Oil temperature | °C |
| $\Lambda$ | Specific film thickness | - |
| $\mu$ | Coefficient of friction | - |
| $\mu_{EHL}$ | Fluid coefficient of friction | - |
| $\mu_{EHL,R}$ | Reference fluid coefficient of friction | - |
| $\mu_F$ | Boundary coefficient of friction for Doleschel model | - |
| $\mu_{F,R}$ | Reference boundary coefficient of friction | - |
| $\mu_{bl}$ | Boundary coefficient of friction for SFK model | - |
| $\mu_{mZ}$ | Average coefficient of friction | - |
| $\mu_{sl}$ | Sliding coefficient of friction | - |
| $\nu$ | Kinematic viscosity | $m^2/s$ |
| $\xi$ | Portion of fluid film friction | - |
| $\rho$ | Oil density | $kg/m^3$ |
| $\rho_0$ | Oil density at 15°C | $kg/m^3$ |
| $\rho_C$ | Equivalent radius of curvature at the pitch point | m |
| $\phi_{bl}$ | Weighting factor for the sliding coefficient of friction | - |
| $\phi_{ish}$ | Inlet shear heating reduction factor | - |
| $\phi_{rs}$ | Kinematic replenishment/starvation reduction factor | - |
| $\omega$ | Angular speed | rad/s |

**Note:** The variables units are presented according to the International System of Units (SI). Throughout the text other units may be used to allow an easier interpretation.

# Contents

# List of Figures

# List of Tables

# CHAPTER 1

# Introduction

## 1.1 Problem Statement and Purpose

Environmental issues have been gaining greater relevance over the years all across the world. Strategic measures have been taken with the goal of creating a more sustainable world in terms of energy usage. The growing introduction of renewable energy sources on our daily lives instead of fossil fuels seems to be the answer. On that matter, the most significant source of renewable energy in the European Union is wind power, which already represents the third greatest energy source as may be seen in figure 1.1.

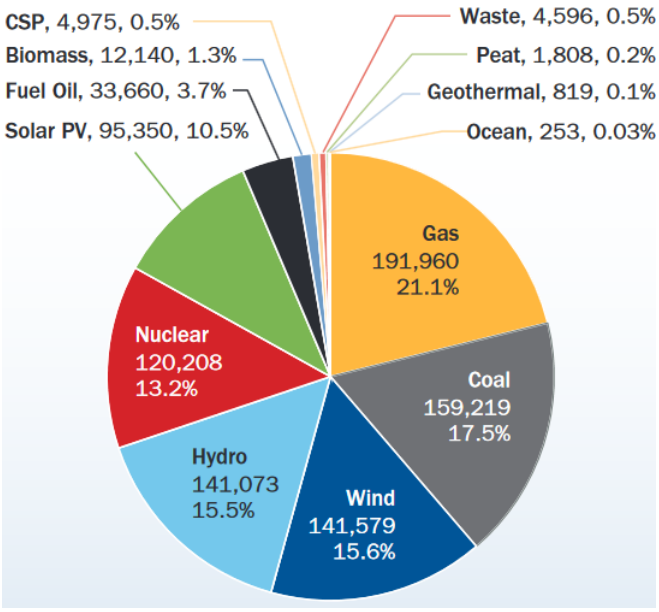


Figure 1.1: Power generation in the EU in 2014, in MW [5].

The energy produced by wind turbines has been increasing every year through the introduction of best performance components and the production of larger diameter turbines.

Although wind power production doesn't represent one of the main energy sources at a world level, in figure 1.2 it's possible to see the growth on its importance until the year of 2015.

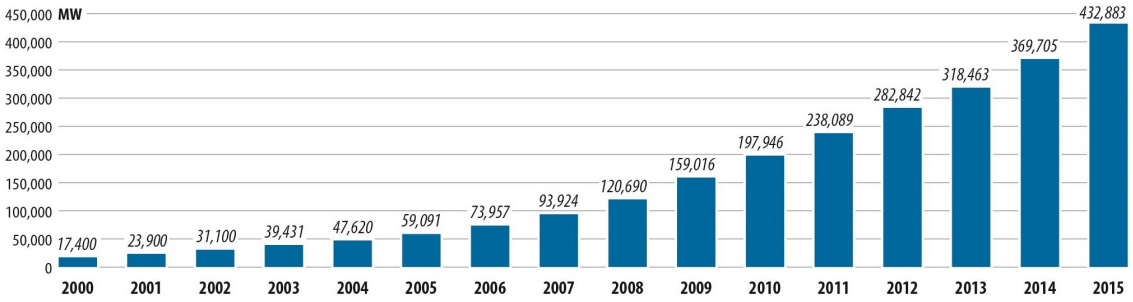


Figure 1.2: Wind power generation worldwide [6].

Since the year of 2000, wind power installations have been increasing at a positive rate, with the exception of the year of 2013 as it is shown in figure 1.3.

In the European Union alone a 12 800 MW of wind power capacity was installed and grid-connected during 2015, an increase of 6.3% on the previous year. There is now 142 GW of installed wind power capacity in the EU: approximately 131 GW onshore and 11 GW offshore. In 2015 wind turbines accounted for 44.2% of total 2015 power plant installations which is more than any other source [5].

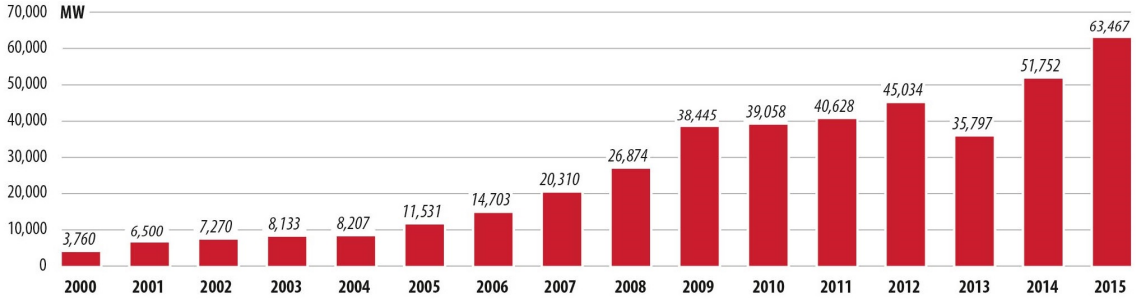


Figure 1.3: Wind power growth worldwide [6].

The blades in the wind turbines are designed to spin as the air flows through them, converting the kinetic energy of the wind into mechanical energy – torque, which is transmitted along the main shaft to the generator through a transmission system as represented in detail in figure 1.4. The rotor rotational speed and torque are transformed by the main gearbox in order to match the necessary operating conditions of the generator. Since very high power levels are involved in this transformation a small change in efficiency per stage on the gearbox can amount to significant overall gains [7, 8].

Planetary gearboxes allow both a compact design and a significant gear ratio making them an interesting option against the use of a regular gearbox with multiple gear stages. One of the applications where planetary gearboxes can be used are the wind turbines to transform the low speed of the spinning blades to the one needed in the input shaft of the generator to produce electricity. Since the power level in these equipments can go up to 10 MW it's easily understood why any increase of efficiency can't be neglected. In order to improve gearbox efficiency the power loss mechanisms need to be studied and understood.

Optimizing gearbox efficiency also leads to lower operating temperature which benefits the working life of all components. Lower operating temperatures lead to a lower failure probability, therefore lowering the maintenance costs [9].

We can divide gearbox power losses in two components: load dependent losses and no-load

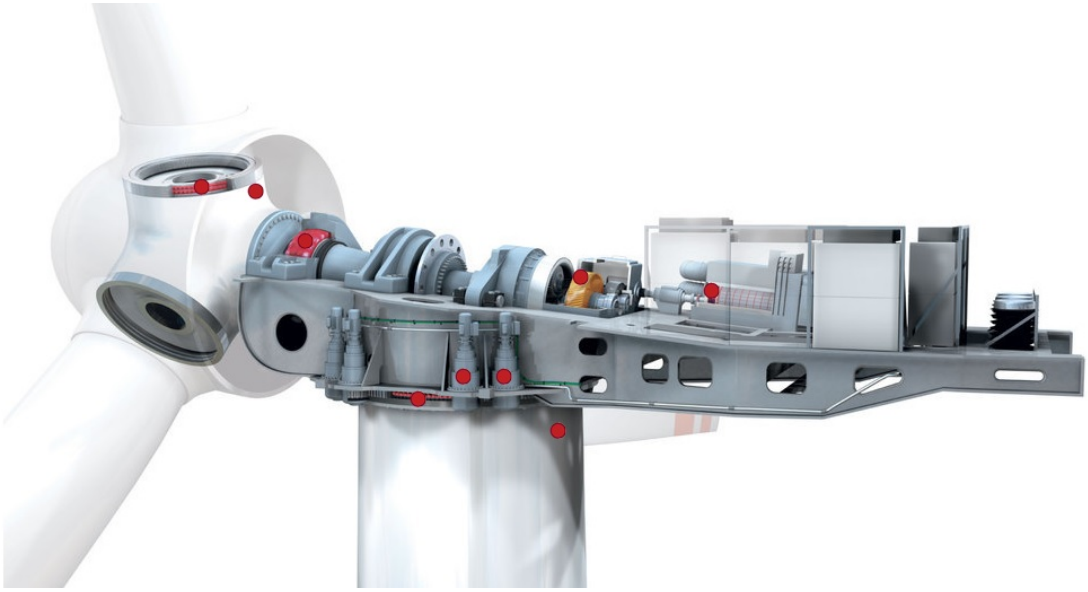

Figure 1.4: Details of the wind turbine transmission system [10].

losses. In this work the interest lays in studying the no-load power losses, in particularly the churning losses.

The importance of churning losses in the total power loss, the constant pursuit of greater efficiency and the lack of correct prediction to this type of losses makes this work challenging and interesting. Some of the no-load losses components have already been studied and are extensively described in literature but for churning losses the proposed models aren't very consistent, as it will be demonstrated in chapter 2. Churning losses are a no-load loss component and they depend on the geometry of the gearbox and its mechanical components like the planet carrier, viscosity and density of the lubricant, and the lubrication method.

In former studies no-load power losses analysis have already been done using numerical and theoretical approaches. However, it doesn't seem to exist coherent results, due to the chaotic nature of the churning phenomenon.

Many studies have been carried on concerning wind turbines. Fernandes *et al.* studied the torque loss on rolling bearings [11] and gears [12] for several wind turbine gear oils. Finally the referred studies where applied to a planetary and a parallel axis gearbox [2], both in multiplying configuration, joining to the work of Pereira [13], for low torque and high rotational speed conditions. Recently, this analysis was made for gearboxes used in wind turbines [7, 8].

Marques *et al.* [3] studied the overall efficiency of a planetary gearbox, for low rotational speed and high torque conditions. This report will be the continuation of the mentioned studies, responding to the necessity of measuring with greater precision the no-load power losses and studying churning losses for a planetary gearbox.

## 1.2 Document Outline

This Dissertation is divided in nine Chapters.

Chapter 2, Gear Churning Loss Models, shows the inherent difficulty when studying churning torque losses comparing four different models from the literature for one given example.

In Chapter 3, Planetary Gearbox Power Loss, the power loss for one gearbox is described presenting the most suitable model for each component of the studied planetary gearbox.

Chapter 4, entitled Experimental Analysis , is dedicated to describe the lubricants properties and the planetary gearbox. The gearbox test rig is shown in detail and the test planning and experimental procedure for the no-load experiments are presented.

The experimental results are presented in Chapters 5, 6 and 7 . Firstly, in No-Load Loss, the no-load torque loss measurements are shown, complementing the results obtained by Camacho [14], and its distribution for each gearbox component is analyzed. Then, churning phenomenon is explored after a set of experiments for a broad range of temperature in Chapter Churning Power Loss. Finally, in Chapter Global Power Loss, the obtained results are applied to a model developed by Marques *et al.* [3] and the total power loss in a planetary gearbox is studied.

The final chapters of this report, Conclusions and Future Works, are dedicated to take the necessary conclusions about the work and future work suggestions, respectively.

# CHAPTER 2

## Gear Churning Loss Models

Articles are easily found in literature on the influence of the churning phenomenon on the efficiency of many types of gears under different conditions. Despite that fact, the results often don't support each other because of the difficulty inherent to the complex study of churning. Even with the use of numerical methods like *CFD* codes and models, the results are repeatedly far from what is obtained in reality.

The first one to try to understand the churning power loss phenomenon was Von Kármán, who did a theoretical analysis on the problem of a flow on a rotating disk immersed in a 'infinite' mass of fluid, in 1946 [15].

Later Daily and Neece [16], and Mann and Marston [17] extended Von Kármán's study with the consideration of an enclosure.

After that, jet and dipped lubrication were experimentally studied. The last one, where the rotating body is only partially immersed, suffered a great development with the contributions of Boness [18], Terekhov [19] and Höhn *et al.* [20]. All of these analyses were made under a large range of operating conditions.

Other authors like Luke and Olver [4], carried out experimental measurements and then compared them with the results obtained by the authors referred above.

Changenet [21] studied the regimes under which the flow occurs in different conditions. Talbot *et al.* [22] tried to understand the effect of helical gear tooth on the results of pocketing power loss.

Over the last few years numerical codes have been applied to the problem under consideration. Concli *et al.* [23] and Marques [24] have shown results for the churning problem on one pair of gears and the planet carrier of a planetary gearbox, respectively, but due to the complexity of the problem it is needed to take in account a lot of simplifications which compromise the final result.

Therefore, the best way to understand this phenomenon seems to be by means of experimental testing. Maybe in the future computer aided models will become more important in these studies but so far, the number of variables and effects to take into consideration is so high that the results rarely correspond to a good prediction.

On a planetary gearbox, churning power losses will not have only in account the losses induced by the complexity of the flow due to the gear meshing but also the presence of the planet carrier, which only increases the difficulty of the problem in hand.

## 2.1 Models Presentation

In order to understand how difficult it is to study churning losses, four models that were referred above are now presented in more detail. After that, they are compared considering the same operating conditions, *i.e.*, same gear and lubrication properties. The objective of this study is to show how complex it is to model the churning problem and on the other hand how dependent it is on the geometry of the enclosure.

The presented models, from the authorship of Boness [18], Terekhov [19], Höhn *et al.* [20] and the most recent from Changenet [21], are on a time line that goes from 1989 all the way to 2011.

Each model determines a torque coefficient ($C_M$ or $C_m$) that allows the calculation of the churning torque ($M_C$).

### 2.1.1 Boness Model

The Boness model [18] refers to three different flow regimes.

For 'laminar' flow ($Re < 2000$) it gives:

$$C_M = \frac{20}{Re} \tag{2.1.1}$$

For 'intermediate' values of Reynolds number ($2000 < Re < 10000$):

$$C_M = 8.6 \times 10^{-4} Re^{1/3} \tag{2.1.2}$$

In a 'turbulent' regime ($Re > 10000$), $C_M$ is given by:

$$C_M = \frac{5 \times 10^8}{Re^2} \tag{2.1.3}$$

For this model, the torque coefficient, $C_M$, and Reynolds number are calculated according to equations (2.1.4) and (2.1.5), respectively.

$$C_M = \frac{2M_C}{\rho \omega^2 R_p^3 A} \tag{2.1.4}$$

$$Re = \frac{\omega R_p L}{\nu} \tag{2.1.5}$$

### 2.1.2 Terekhov Model

Terekhov [19] also suggests that the flow can by divided in three different zones. For the first one ($Re^{-0.6} Fr^{-0.75} < 8.7 \times 10^{-3}$ and $Re < 2250$) it comes:

$$C_M = 4.75 Re^{-0.6} Fr^{-0.25} \times \left(\frac{V_1}{V_m}\right)^{-0.3} \left(\frac{V_\epsilon}{V_m}\right)^{-0.2} \left(\frac{b}{R_a}\right)^{-0.4} \left(\frac{d_i}{R_a}\right)^{1.5} \tag{2.1.6}$$

In the intermediate zone ($Re^{-0.6}Fr^{-0.75} > 8.7 \times 10^{-3}$ and $Re < 2250$), $C_M$ is calculated by:

$$C_M = 2.63Re^{-0.6}Fr^{-0.25} \times \left(\frac{V_1}{V_m}\right)^{-0.53}\left(\frac{V_\epsilon}{V_m}\right)^{-0.2}\left(\frac{b}{R_a}\right)^{-0.4}\left(\frac{d_i}{R_a}\right)^{1.5} \tag{2.1.7}$$

For the final region ($Re > 2250$) one has:

$$\begin{aligned} C_M = 0.97Re^{-0.6}Fr^{-[0.464+0.037(R_a/d_i]} \times \left(\frac{V_1}{V_m}\right)^{-0.376} \\ \times \left(\frac{V_\epsilon}{V_m}\right)^{-0.2}\left(\frac{b}{R_a}\right)^{-0.124}\left(\frac{d_i}{R_a}\right)^{0.37} \end{aligned} \tag{2.1.8}$$

In Terekhov model [19] the torque coefficient, Froude and Reynolds numbers are given by, respectively:

$$C_M = \frac{M_C}{\rho\omega^2 R_a^4 b} \tag{2.1.9}$$

$$Fr = \frac{\omega^2 R_a}{g} \tag{2.1.10}$$

$$Re = \frac{\omega R_a^2}{\nu} \tag{2.1.11}$$

### 2.1.3 Höhn Model

For the model developed by Höhn [20], one has to take into consideration that the calculations are made for one pair of gears instead of just one pinion like the previous models.

The churning torque, $M_C$, is given by:

$$M_C = C_{Sp}C_1 e^{C_2(v_t/10\ \mathrm{m/s})} \tag{2.1.12}$$

Where the constants are calculated by the following equations:

$$C_1 = 0.063\left(\frac{d_{i_1} + d_{i_2}}{10\ \mathrm{mm}}\right) + 0.0128\left(\frac{b}{10\ \mathrm{mm}}\right)^3 \tag{2.1.13}$$

$$C_2 = \frac{d_{i_1} + d_{i_2}}{800\ \mathrm{mm}} + 0.2 \tag{2.1.14}$$

$$C_{Sp} = \left(\frac{2R_{a_2}}{l_H}\right)\left(\frac{4d_{i_2}}{3R_{a_2}}\right)^{1.5} \tag{2.1.15}$$

The constant $l_H$ is calculated through equation (2.1.16).

$$l_H = \frac{2(L_{Hohn}H_{Hohn})}{L_{Hohn} + H_{Hohn}} \tag{2.1.16}$$

### 2.1.4 Changenet Model

Changenet [21] also created a model for churning torque prediction for one pinion. The equations for calculating the dimensionless drag torque, $C_m$, depend on the acceleration, $\gamma$, and critical Reynolds number, Rec, and are the result of dimensional analysis.

For values of $\gamma < 750$ m/s$^2$ and $Rec < 4000$, the dimensionless drag torque, $C_m$, is given by:

$$C_m = 1.366\left(\frac{d_i}{D_p}\right)^{0.45}\left(\frac{V_m}{D_p^3}\right)^{0.1} Fr^{-0.6} Rec^{-0.21}\left(\frac{b}{R_p}\right)^{0.21} \tag{2.1.17}$$

If $\gamma < 750$ m/s$^2$ and $Rec > 4000$, $C_m$ comes:

$$C_m = 0.239\left(\frac{d_i}{D_p}\right)^{0.45}\left(\frac{V_m}{D_p^3}\right)^{0.1} Fr^{-0.6}\left(\frac{b}{R_p}\right)^{0.21} \tag{2.1.18}$$

For $\gamma > 1250$ m/s$^2$ and $Rec < 4000$, one has:

$$C_m = 20.797\left(\frac{d_i}{D_p}\right)^{0.1}\left(\frac{V_m}{D_p^3}\right)^{-0.35} Fr^{-0.88} Rec^{-0.21}\left(\frac{b}{D_p}\right)^{0.85} \tag{2.1.19}$$

For the final condition ($\gamma > 1250$ m/s$^2$ and $Rec > 4000$), the dimensionless drag torque is calculated by equation (2.1.20):

$$C_m = 3.644\left(\frac{d_i}{D_p}\right)^{0.1}\left(\frac{V_m}{D_p^3}\right)^{-0.35} Fr^{-0.88}\left(\frac{b}{D_p}\right)^{0.85} \tag{2.1.20}$$

Critical Reynolds number, $Rec$, acceleration, $\gamma$, and Froude number, $Fr$, are calculated with equations (2.1.21), (2.1.22) and (2.1.23), respectively.

$$Rec = \frac{\omega R_p b}{\nu} \tag{2.1.21}$$

$$\gamma = \omega^2 (R_p b m)^{1/3} \tag{2.1.22}$$

$$Fr = \frac{\omega^2 R_p}{g} \tag{2.1.23}$$

After obtaining the value of dimensionless drag torque, $C_m$, churning torque comes:

$$M_C = \frac{1}{2}\rho\omega^2 R_p^3 A C_m \tag{2.1.24}$$

## 2.2 Models Comparison

For the same gear pair, with two equal pinions, under the same conditions the models of Boness [18], Terekhov [19], Höhn [20] and Changenet [21] were tested to calculate the values of churning torque loss. The parameters of the case in study are presented in table 2.1. The oil's physical and chemical properties correspond to the ones of PAOR at 70 °C, one of the tested gear oils presented in table 4.1. The dimensions of the 'box' considered for Höhn [20] model were both 200 mm for $L_{Hohn}$ and $H_{Hohn}$. The results are presented in the figure 2.1.

For the models of Boness [18], Terekhov [19] and Changenet [21] the results were multiplied by 2 to account for a gear pair instead of just one pinion. Although this may seem a rough approximation it was only considered to allow a comparison on the prediction for each one of the models.

Table 2.1: Gear parameters and lubrication properties for the gear churning loss simulations.

| | | | | |
|---|---|---|---|---|
| **Gear Parameters** | $R_p$ /mm | $b$ /mm | $z$ /- | $m$ /mm |
| | 32 | 20 | 32 | 2 |
| **Lubrication Properties** | $\nu$ /cSt | $\rho$ /kg/m$^3$ | $V_m$ /dm$^3$ | $d_i$ /mm |
| | 84.9829 | 0.8325 | 2 | 10 |

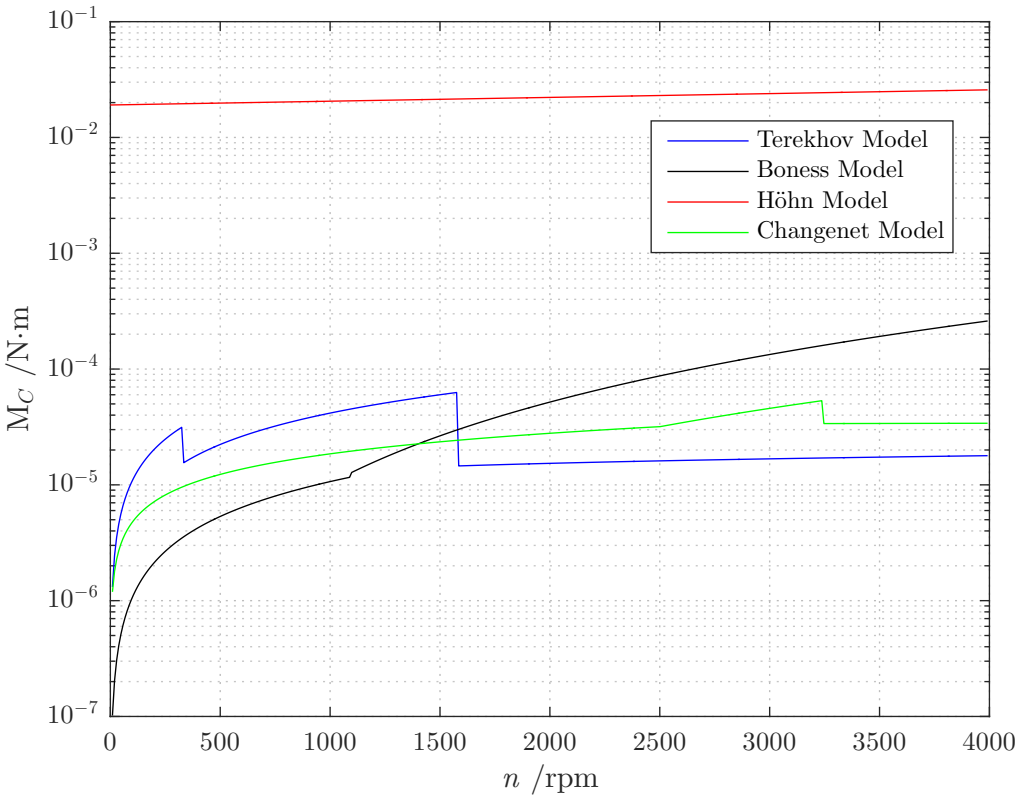


Figure 2.1: Churning torque comparison using different models.

The churning torque variation with rotational speed presents a great discrepancy for the different models tested. In fact, a logarithmic scale is needed to be able to represent them all in the same figure. The models of Terekhov [19] and Changenet [21] present a few similarities but one can't say with certainty that these models are the accurate ones for the case in study.

The churning loss models are based on empirical studies where a model based on a non-dimensional analysis is adjusted. Each author used different oils in housings with different enclosures. Just that last factor changes the way the oil flows and the viscous dissipation will be different. So, one may be able to create a model to predict churning, but theoretically, that will work alone for one enclosure. In other words, if only the rotation speed and lubricant (properties) are different, it is possible to think of a correlation between them and churning torque loss.

# CHAPTER 3

# Planetary Gearbox Power Loss

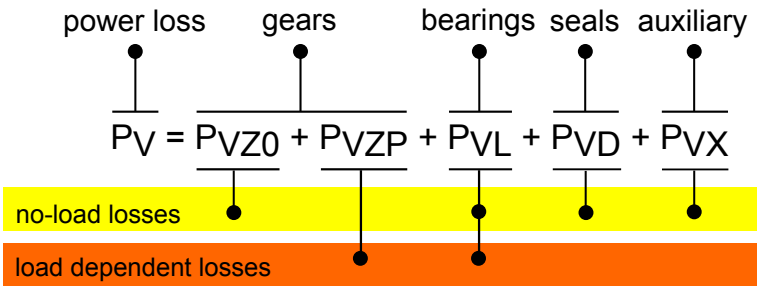


Figure 3.1: Power loss components in a gearbox according to Höhn *et al.* [25].

The total power loss in a gearbox is described in figure 3.1. This equation is also applicable for a planetary configuration. Every component will contribute in different manners for the overall power loss. We can divide it in load and no-load losses. Generally, load dependent losses are more important than no-load losses. However, if operating conditions correspond to high rotation speeds and/or low loads, the load independent losses may become the most important component to take under consideration.

Load losses depend mainly on the load condition imposed to the gearbox. So, they are affected mostly by the power transmitted by each component and the coefficient of friction. This losses are promoted by gears and bearings.

Load independent losses are a function of kinematic conditions, namely the rotation speed, oil properties as density and viscosity and lubrication method. Gears, bearings and shaft seals contribute to this kind of losses. In a planetary gearbox, the planet carrier will also influence no-load losses and will be taken into account on the component of auxiliary power losses.

In the following sections the contributions of each one of the mechanical components to the overall power loss will be described according to models proposed by many authors, making a few references to features of the studied planetary gearbox.

## 3.1 Gears Load Power Loss

The load power loss in gears can be calculated through equation (3.1.1), if one considers an average coefficient of friction along the contact path, $\mu_{mZ}$.

$$P_{VZP} = P_{IN} H_V \mu_{mZ} \tag{3.1.1}$$

Many authors modeled the calculation of the gear loss factor, $H_V$, and the average coefficient of friction, $\mu_{mZ}$, and here are some examples found in literature.

### 3.1.1 Gear Loss Factor

#### Ohlendorf

The model proposed by Ohlendorf [26] for the calculation of the gear loss factor is given by:

$$H_V^{Ohl} = (1+u)\frac{\pi}{z_1}\frac{1}{u \cdot \cos\beta_b}(1 - \epsilon_\alpha + \epsilon_1^2 + \epsilon_2^2) \tag{3.1.2}$$

He then proposed a model for a wider range of gears, in equation (3.1.3).

$$H_V^{OhlM} = \frac{\pi(u+1)}{z_1 \cdot u\cos(\beta_b)}\left(a_0 + a_1|\epsilon_1| + a_2|\epsilon_2| + a_3|\epsilon_1|\epsilon_1 + a_4|\epsilon_2|\epsilon_2\right) \tag{3.1.3}$$

Three parameters are defined based on $\epsilon_1$, $\epsilon_2$ and $\epsilon_\alpha$:

- $l_1$ - Round up to the nearest positive integer ($\epsilon_1$);
- $m_1$ - Round up to the nearest positive integer ($\epsilon_2$);
- $n_1$ - Round up to the nearest positive integer ($\epsilon_\alpha$).

Based on these parameters, $a_0$ to $a_4$ coefficients are calculated according to table 3.1.

Table 3.1: Values for the $a_i$, $(i = 0:4)$, coefficients of equation 3.1.3.

| | $\epsilon_\alpha < 1$ | $\epsilon_\alpha > 1$<br>$\epsilon_1 < 0 \vee \epsilon_2 < 0$ | $\epsilon_\alpha > 1$<br>$\epsilon_1, \epsilon_2 > 0$<br>$l_1 + m_1 = n_1$ | $\epsilon_\alpha > 1$<br>$\epsilon_1, \epsilon_2 > 0$<br>$l_1 + m_1 = n_1 + 1$ |
|---|---|---|---|---|
| $a_0$ | 0 | 0 | $\frac{2l_1m_1}{n_1}$ | $\frac{2(l_1m_1-n_1)}{n_1-1}$ |
| $a_1$ | 0 | 1 | $\frac{l_1(l_1-1)-m_1(m_1-1)-2l_1m_1}{n_1(n_1-1)}$ | $\frac{l_1(l_1-1)+m_1(m_1-1)-2(m_1-1)n_1}{n_1(n_1-1)}$ |
| $a_2$ | 0 | 1 | $\frac{-l_1(l_1-1)+m_1(m_1-1)-2l_1m_1}{n_1(n_1-1)}$ | $\frac{l_1(l_1-1)+m_1(m_1-1)-2(m_1-1)n_1}{n_1(n_1-1)}$ |
| $a_3$ | $\frac{1}{\epsilon_\alpha}$ | 0 | $\frac{2m_1}{n_1(n_1-1)}$ | $\frac{2(m_1-1)}{n_1(n_1-1)}$ |
| $a_4$ | $\frac{1}{\epsilon_\alpha}$ | 0 | $\frac{2l_1}{n_1(n_1-1)}$ | $\frac{2(l_1-1)}{n_1(n_1-1)}$ |

#### Niemann

Niemann and Winter [27] proposed another solution.

$$H_V^{Nie} = (1+u)\frac{\pi}{z_1}\frac{1}{\cos\beta_b}\epsilon_\alpha\left(\frac{1}{\epsilon_\alpha} - 1 + (2k_0^2 + 2k_0 + 1)\epsilon_\alpha\right) \tag{3.1.4}$$

Where $k_0$ is defined by equation (3.1.5).

$$k_0 = \frac{z_1}{2\pi \cdot \epsilon_\alpha \cdot u} \left( \left( \left( \frac{R_{a_2}}{R_{p_2}} \right)^2 \frac{1}{\cos \alpha_t^2} - 1 \right)^{\frac{1}{2}} - \tan \alpha_t \right) \tag{3.1.5}$$

**Buckingham**

Buckingham [28] also introduced a model for the gear loss factor given by equation (3.1.6).

$$H_V^{Buc} = (1+u)\frac{\pi}{z_1}\frac{1}{\cos \beta_b}\epsilon_\alpha(2k_0^2 + 2k_0 + 1) \tag{3.1.6}$$

### 3.1.2 Coefficient of Friction

The coefficient of friction is a parameter very complex to model as it is not only dependent on the lubricant physical and chemical properties, but also on macro and micro geometric features of the surfaces in contact and the load distribution.

Mainly due to the complexity of this problem, most of the models for the calculation of $\mu(x, y)$ are based in equations that are fitted to numerical or experimental data, being one more adequate than others depending on the lubrication regime.

**Kelley-Lemanski**

Kelley and Lemanski [29] derived an equation for the coefficient of friction from experiments in twin disc machines. The authors also validated their results for meshing gears, with the restriction of not being applicable to calculate the evolution of the coefficient of friction along the contact path.

$$\mu_{mZ} = 0.0127 \cdot \log_{10}\left( \frac{F_{bt}}{b} \cdot \frac{29652}{\eta \cdot v_g \cdot v_{\Sigma C}^2} \right) \tag{3.1.7}$$

**Michaelis**

Michaelis *et al.* [30] proposed the equation (3.1.8) to predict the average coefficient of friction between gear teeth. Compared to equation (3.1.7) this approach introduces the influence of the average roughness, $Ra$.

$$\mu_{mZ} = 0.045 \cdot \left( \frac{F_{bt}/b}{v_{\Sigma C} \cdot \rho_C} \right)^{0.2} \eta^{-0.05} \cdot X_R \tag{3.1.8}$$

Where $X_R$ is given by equation (3.1.9).

$$X_R = 8.8 \cdot \sqrt[4]{\frac{Ra}{D_p}} \tag{3.1.9}$$

### Schlenk

Schlenk [31] adapts the solution proposed by Michaelis to account for different lubricant formulations with the introduction of the lubricant parameter, $X_L$, and it follows in equation (3.1.10).

$$\mu_{mZ} = 0.048 \cdot \left( \frac{F_{bt}/b}{v_{\Sigma C} \cdot \rho_C} \right)^{0.2} \cdot \eta^{-0.05} \cdot Ra^{0.25} \cdot X_L \tag{3.1.10}$$

Values of the lubricant parameter for the tested gear oils, presented in table 4.1, are shown in table 3.2.

Table 3.2: $X_L$ values for the tested gear oils [32].

| Oil | $X_L$ |
|---|---|
| PAOR | 0.666 |
| MINR | 0.858 |
| MINE | 0.746 |
| PAGD | 0.572 |

This model was the one used by Marques *et al.* [3] and Fernandes *et al.* [12] for the prediction of the power loss in the gears.

### ISO 6336

The formula proposed by ISO [33], equation (3.1.11), usually yields higher values than the expected for the coefficient of friction. This formula has the same structure, yet different exponents, as the ones proposed by the authors referred above.

$$\mu_{ISO} = 0.143 \cdot \left[ \frac{F_N/b \cdot R_a}{\rho_C \cdot \eta \cdot v_{\Sigma C}} \right]^{\frac{1}{4}} \tag{3.1.11}$$

### Doleschel

Doleschel [34] defined the coefficient of friction in a gear mesh as a combination of the boundary film, $\mu_F$, and fluid film friction, $\mu_{EHL}$.

The average coefficient of friction, $\mu_{mZ}$, is then calculated as a weighted linear combination of the boundary and fluid film lubrication based on the analysis of the specific film thickness, $\Lambda$. The weight factor, $\xi$, is set as the portion of fluid friction.

$$\mu_{mZ} = (1 - \xi) \cdot \mu_F + \xi \cdot \mu_{EHL} \tag{3.1.12}$$

The portion of fluid film friction, $\xi$, depends on the specific film thickness, $\Lambda$, in the contact as represented by equation (3.1.13).

$$\xi = \begin{cases} \Lambda - 0.25 \cdot \Lambda^2, \ for\ \Lambda < 2 \\ \\ 1, \ for\ \Lambda \geq 2 \end{cases} \tag{3.1.13}$$

The boundary coefficient of friction and the fluid coefficient of friction can be calculated according to equations (3.1.14) and (3.1.15), respectively.

$$\mu_F = \mu_{F,R} \cdot \left(\frac{p_H}{p_R}\right)^{\alpha_F} \cdot \left(\frac{V_\Sigma}{V_{R,F}}\right)^{\beta_F} \tag{3.1.14}$$

$$\mu_{EHL} = \mu_{EHL,R} \cdot \left(\frac{p_H}{p_R}\right)^{\alpha_{EHL}} \cdot \left(\frac{V_\Sigma}{V_{R,EHL}}\right)^{\gamma_{EHL}} \tag{3.1.15}$$

The exponents in equations (3.1.14) and (3.1.15) are derived from experimental data.

**Xu Hai**

Xu Hai [35] proposed a coefficient of friction based on results obtained with an EHL model (numerical results) that was validated with experimental traction curves.

$$\mu_{Xu} = e^{f(SR,P_h,\eta,S)} P_h^{b2} |SR|^{b3} V_e^{b6} \nu^{b7} R^{b8} \tag{3.1.16}$$

$$f(SR, P_h, \eta, S) = b_1 + b_4 |SR| P_h log_{10}(\eta) + b_5 e^{-|SR|P_h log_{10}(\eta)} + b_9 e^S \tag{3.1.17}$$

The coefficients, from $b_1$ to $b_9$, that go into equations (3.1.16) and (3.1.17) are presented in table 3.3.

Table 3.3: Coefficients for the EHL based formula [35].

| | |
|---|---|
| $b_1$ | -8.916465 |
| $b_2$ | 1.03303 |
| $b_3$ | 1.036077 |
| $b_4$ | -0.354068 |
| $b_5$ | 2.812084 |
| $b_6$ | -0.100601 |
| $b_7$ | 0.752755 |
| $b_8$ | -0.390958 |
| $b_9$ | 0.620305 |

## 3.2 Gears No-Load Power Loss

The gears produce power loss even when they are not submitted to a load condition. This is due to the flow induced by the rotation of the gears which leads to viscous dissipation in the lubricant creating a mechanism of churning power loss.

As it was explained in detail in Chapter 2, this power loss component, $P_{VZ0}$, may be affected by rotation speed, lubrication properties and gearbox design. Churning losses can represent an important source of energy dissipation for very high speeds and/or low loads. As the gears present a complex geometry, the flow generated by its rotation as a very chaotic profile. So, it is hard to develop an equation for the prediction of this power loss component. Experimental data seems to be the only way, so far, of quantifying the losses due to this phenomenon.

For a planetary gearbox the problem presents other difficulty relatively to a gear pair because it is necessary to consider the interaction between each planet and the sun and ring gears.

## 3.3 Bearings Power Loss

Bearings are the mechanical components which support the loads transmitted by the gears through the shafts and they are usually one of the main power loss sources in a gearbox. Each type of bearing contributes on its on way to secure the operating conditions of the gearbox. Depending on the bearing type, the power loss is modeled through different equations, usually given by its manufacturers but also available in literature. In the tested planetary gearbox there are three types of bearings:

- Deep groove ball bearings;
- Tapered roller bearings;
- Full-complement needle roller bearings.

Two SKF models [36, 37] are now presented to calculate the power loss for these mechanical components.

Despite of its general calculation being presented, deep groove ball bearings were not taken into consideration since the tests were performed under no-load conditions and the tapered roller bearings have a quite large pre-load applied, thus rendering the deep groove ball bearings losses negligible. Both full-complement needle and tapered roller bearings contribute to a load independent loss. The influence of the last one is almost exclusively due to the pre-load at which they are submitted. The speeds at which they operate was already presented in chapter 4.2.

### 3.3.1 SKF Model, 2013

To take in account the power loss in tapered roller bearings, *SKF Rolling Bearings Catalogue 6000 EN* [36] is described. None the less, most of the formulas presented are also applicable to deep groove ball bearings. Generally, these bearings can generate much higher power loss than the rest, and those losses vary substantially with the pre-load.

To accurately calculate the total frictional torque in a roller bearing, the following tribological effects must be considered:

- Rolling frictional torque and eventual effects of high-speed starvation and inlet shear heating;
- Sliding frictional torque and its effect on the quality of lubrication;
- Frictional torque from seals;
- Frictional torque from drag losses, churning, splashing, etc.

The total power loss in a bearing, presented in equation (3.3.1), is directly proportional to the rotation speed and frictional torque.

$$P_{VL} = M \cdot n \cdot \frac{\pi}{30} \times 10^{-3} \tag{3.3.1}$$

The frictional torque is calculated according to equation (3.3.2).

$$M = M_{rr} + M_{sl} + M_{seal} + M_{drag} \tag{3.3.2}$$

### Rolling Frictional Torque

The rolling frictional torque, $M_{rr}$, is given by:

$$M_{rr} = \phi_{ish} \cdot \phi_{rs} \cdot G_{rr} \cdot (\nu \cdot n)^{0.6} \tag{3.3.3}$$

The inlet shear heating reduction factor, $\phi_{ish}$, takes in account that only a tiny amount of lubricant is used to form a hydrodynamic film. Therefore, some of the oil close to the contact area inlet is rejected and produces a reverse flow, as seen in figure 3.2. This reverse flow shears the lubricant, generating heat, which lowers the oil viscosity and reduces the film thickness and rolling friction.

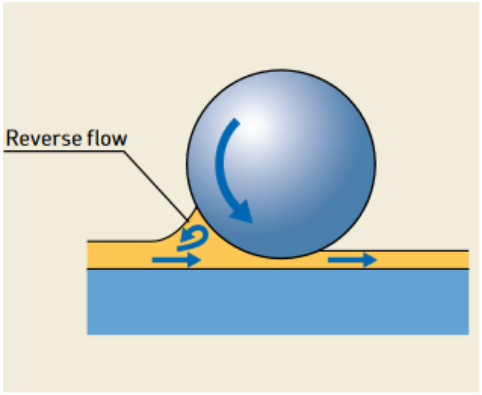


Figure 3.2: Reverse flow in a ball bearing [36].

The kinematic replenishment/starvation reduction factor, $\phi_{rs}$, considers applications where viscosity or speeds are high. As a result, the lubricant may not have sufficient time to replenish the raceways, causing a 'kinematic starvation' effect, which reduces the thickness of the hydrodynamic film and rolling friction.

The inlet shear heating reduction factor, $\phi_{ish}$, and kinematic starvation reduction factor, $\phi_{rs}$, are presented in equations (3.3.4) and (3.3.5), respectively.

$$\phi_{ish} = \frac{1}{1 + 1.84 \cdot 10^{-9} \cdot (n \cdot d_m)^{1.28} \cdot \nu^{0.64}} \tag{3.3.4}$$

$$\phi_{rs} = \frac{1}{e^{K_{rs} \cdot \nu \cdot (d+D)} \cdot \sqrt{\frac{K_z}{2 \cdot (D-d)}}} \tag{3.3.5}$$

$G_{rr}$, for tapered roller bearings, is calculated through the following equation:

$$G_{rr} = R_1 \cdot d_m^{2.38} \cdot (Fr + R_2 \cdot Y \cdot F_a)^{0.31} \tag{3.3.6}$$

The pre-load, $F_a$, was estimated to be 4.66 kN, the minimum to secure proper operating conditions.

### Sliding Frictional Torque

The sliding frictional torque, $M_{sl}$, comes:

$$M_{sl} = G_{sl} \cdot \mu_{sl} \tag{3.3.7}$$

For tapered roller bearings, $G_{sl}$ is calculated by equation (3.3.8).

$$G_{sl} = S_1 \cdot d_m^{0.82} \cdot (F_r + S_2 \cdot Y \cdot F_a) \tag{3.3.8}$$

Where $S_1$ and $S_2$ are geometric constants.

The sliding coefficient of friction, $\mu_{sl}$, is presented in equation (3.3.9).

$$\mu_{sl} = \phi_{bl} \cdot \mu_{bl} + (1 - \phi_{bl}) \cdot \mu_{EHL} \tag{3.3.9}$$

The fluid coefficient of friction, $\mu_{EHL}$, may assume different values:

- 0.02 for cylindrical roller bearings;
- 0.002 for tapered roller bearings ($\mu_{EHL}^{SKF,TRB}$);
- other bearings: 0.05 for mineral oils and 0.04 for synthetic oils ($\mu_{EHL}^{SKF,baseoil}$).

The boundary coefficient of friction is usually $\mu_{bl} = 0.15$.

In previous works [11], the influence of the lubricants used in this work on the $\mu_{sl}$ was investigated for thrust ball and roller bearings. It was concluded that the values of $\mu_{bl}$ and $\mu_{EHL}$ are different for each lubricant and the values presented by SKF are representative of the worst case scenario. To take this into consideration equation (3.3.10) was applied for $\mu_{EHL}$ were the values obtained for thrust roller bearings (the rolling elements are more similar to the ones found in a tapered roller bearing) where compared with the ones given by SKF. The values used for $\mu_{bl}$ are the ones presented in the table 3.4.

Table 3.4: Coefficient of friction of a thrust roller bearing for an operating temperature of 80 °C [11].

| Oil | Parameter | Value |
|---|---|---|
| MINR | $\mu_{bl}$ | 0.035 |
| | $\mu_{EHL}$ | 0.018 |
| PAOR | $\mu_{bl}$ | 0.039 |
| | $\mu_{EHL}$ | 0.010 |
| MINE | $\mu_{bl}$ | 0.044 |
| | $\mu_{EHL}$ | 0.008 |
| PAGD | $\mu_{bl}$ | 0.025 |
| | $\mu_{EHL}$ | 0.010 |

$$\mu_{EHL} = \frac{\mu_{EHL}^{table}}{\mu_{EHL}^{SKF,baseoil}} \times \mu_{EHL}^{SKF,TRB} \tag{3.3.10}$$

The factor $\phi_{bl}$, used for weighting the sliding frictional coefficient is given by equation (3.3.11).

$$\phi_{bl} = \frac{1}{e^{2.6 \cdot 10^{-8} \cdot (\nu \cdot n)^{1.4} \cdot d_m}} \tag{3.3.11}$$

### Frictional Torque from Seals

The frictional moment from seals, $M_{seal}$, is presented in equation (3.3.12).

$$M_{seal} = K_{S1} \cdot d_S^{\beta_1} + K_{S2} \tag{3.3.12}$$

In this particular case, the tapered roller bearings aren't sealed so it comes, $M_{seal} = 0$.

### Frictional Torque from Drag Losses

The frictional torque from drag losses, $M_{drag}$, accounts for the resistance of the rolling elements when moving through the oil and includes the effects of the viscosity of the oil and it's calculated according to equation (3.3.13), with the drag loss factor, $V_M$, obtained from figure 3.3.

$$M_{drag} = 4 \cdot V_M \cdot K_{roll} \cdot C_W \cdot B \cdot d_m^4 \cdot n^2 + 1.093 \cdot 10^{-7} \cdot n^2 \cdot d_m^3 \tag{3.3.13}$$

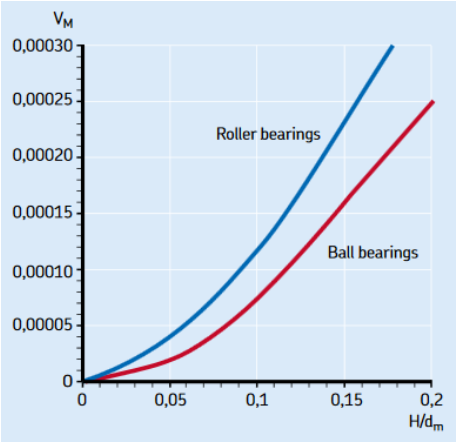


Figure 3.3: Drag loss factor, $V_M$ [36].

$$K_{roll} = \frac{K_L \cdot K_z \cdot (d + D)}{D - d} \cdot 10^{-12} \tag{3.3.14}$$

Where $K_L$ and $K_z$ are geometric constants related to the bearing type.

$$C_W = 2.789 \cdot 10^{-10} \cdot l_D^3 - 2.786 \cdot 10^{-4} \cdot l_D^2 + 0.0195 \cdot l_D + 0.6439 \tag{3.3.15}$$

A few intermediate variables are used and presented in equations (3.3.16), (3.3.17), (3.3.18) and (3.3.19).

$$l_D = 5 \cdot \frac{K_L \cdot B}{d_m} \tag{3.3.16}$$

$$R_S = 0.36 \cdot d_m^2 \cdot (t - sin(t)) \cdot f_A \tag{3.3.17}$$

$$f_A = 0.05 \cdot \frac{K_z \cdot (D + d)}{D - d} \tag{3.3.18}$$

$$t = 2 \cdot cos^{-1}\left(\frac{0.6 \cdot d_m - H}{0.6 \cdot d_m}\right) \tag{3.3.19}$$

Where $H$ is the oil level, represented in figure 3.4.

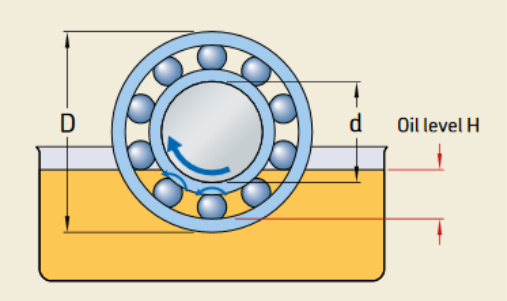


Figure 3.4: Oil level, $H$, schematic [36].

To determine the oil level, $H$, for tapered roller bearings, the lowest point to be considered should be the outside diameter, and for all the other bearings should be the outer ring mean diameter. In the present work, the tests were performed with two oil volumes, 0.75 and 1 L, that correspond approximately to an oil level, $H$, of 20 and 10 mm, respectively.

### 3.3.2 SKF Model, 1981

With the goal of studying the power loss on a full-complement needle roller bearing, *SKF Hauptkatalog Nr. 2800T* [37] was used for needle roller bearings. According to it, the total torque losses are calculated using equation (3.3.20).

$$T_V = T_{VL0} + T_{VLP1} + T_{VLP2} \tag{3.3.20}$$

The load dependent losses, $T_{VLP1}$ and $T_{VLP2}$, are calculated with equations (3.3.21) and (3.3.22).

$$T_{VLP1} = 10^{-3} \cdot f_1 \cdot P_1 \cdot d_m \tag{3.3.21}$$

$$T_{VLP2} = f_2 \cdot F_a \cdot d_m \cdot 10^{-3} \tag{3.3.22}$$

No-load torque losses are given by equation (3.3.23)

$$T_{VL0} = \begin{cases} 1.6 \cdot 10^{-}8 \cdot f_0 \cdot d_m^3 & \text{when } \nu \cdot n < 2000 \\ 10^{-10} \cdot f_0 \cdot (\nu \cdot n)^{\frac{2}{3}} \cdot d_m^3 & \text{when } \nu \cdot n \geq 2000 \end{cases} \tag{3.3.23}$$

For oil sump lubrication, according to [38], one has $f_0 = 12$.

In cageless needle roller bearings, so-called full-complement roller bearings, sliding friction occurs between adjacent rolling elements instead of between rolling elements and cage pockets. This friction exceeds that in the cage pocket, because the sliding motions are in opposite directions [38]. For that matter, Harris [39, 40] suggests that the real torque loss is the torque loss of a needle roller bearing with rolling elements of the same size multiplied by a factor of 1.5 to 2. A factor of 1.75 was selected.

To calculate the power loss one must introduce the result of equation (3.3.23) in equation (3.3.1) but without the factor $10^{-3}$ since the result for $T_{VL0}$ already comes in N·m.

## 3.4 Shaft Seals Power Loss

The power loss produced by shaft seals is often considered independent of the load and the least important component to consider. However, three different models are presented to its prediction. The one that was used in the model development it's the one presented by Simrit [41].

### 3.4.1 Simrit Model

So the seals power loss, $P_{VD}$, is calculated with equation (3.4.1).

$$P_{VD} = 7.69 \times 10^{-6} \times d_{sh}^2 \times n \tag{3.4.1}$$

In figure 3.5, one can see the variation of the seals power loss with two properties, speed and shaft diameter.

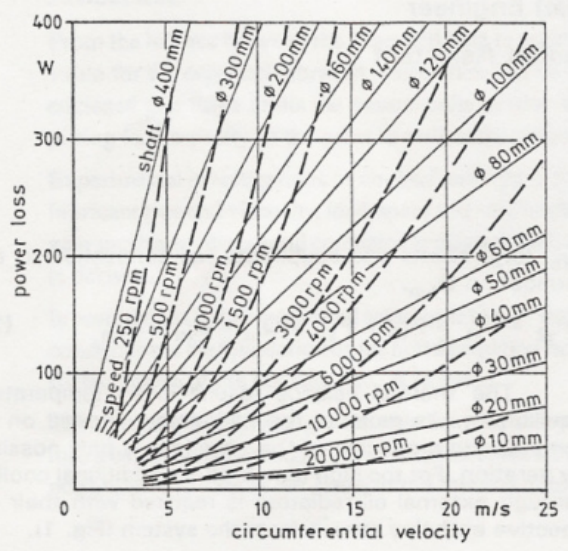


Figure 3.5: Power loss in seals [20].

### 3.4.2 Linke Model

Linke [42] developed other formula taking into account the lubricant viscosity.

$$P_{VD} = [145 - 1.6 \cdot \theta + 350 \log \log(\nu_{40} + 0.8)] \cdot 10^{-7} \cdot d_{sh}^2 \cdot n \tag{3.4.2}$$

### 3.4.3 Kettler Model

Kettler [43] proposed a model where the oil viscosity variation with temperature is considered.

$$P_{VD} = 7.9163 \times 10^{-6} \times F_D \times d_{sh}^2 \times n \tag{3.4.3}$$

Where $F_D$ is a factor that represents the influence of the temperature on the viscosity of the oil.

## 3.5 Auxiliary Power Loss

This component of power loss takes in consideration other losses that aren't accounted for gears, bearings and seals. In the case of the planetary gearbox in specific, the churning promoted by the planet carrier will be discriminated in this component. Naturally, as this phenomenon is very dependent on the shape of the gearbox it's very difficult to predict results.

Marques [24] already did a numerical study with *ANSYS Fluent* on the tested gearbox to try to understand this loss component. However, this results are consequence of a series of approaches that may compromise the final result. One of the performed simulations is presented in figure 3.6, showing the oil flow in the planet carrier.

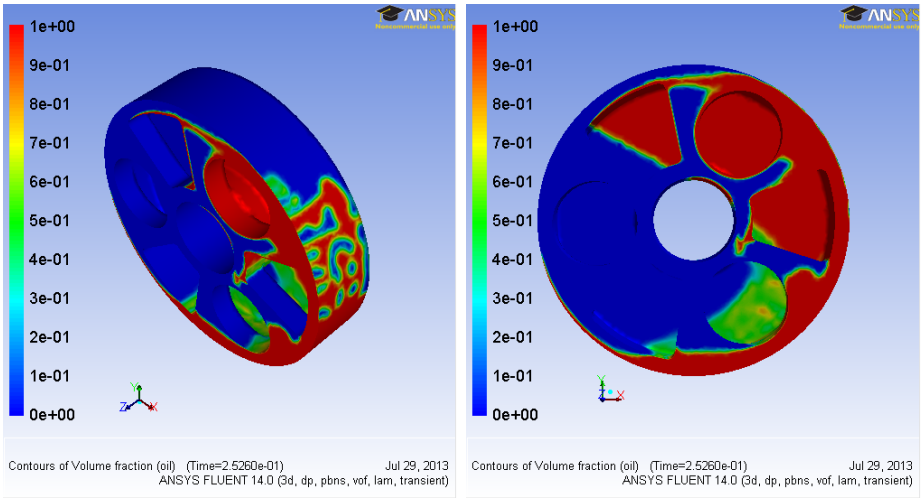


(a) Isometric view. (b) Frontal view.

Figure 3.6: *CFD* simulation to predict churning power loss in the planet carrier [24].

# CHAPTER 4

# Experimental Analysis

## 4.1 Wind Turbine Gear Oils

In order to achieve an efficient behavior of the gearbox, wind turbine gear oils must provide protection both for the gears and bearings, and at the same time be compatible with other components, like the seals. So, there must be a balance between high scuffing resistance and an excellent micro-pitting protection. The lubricant also needs to assure the proper work conditions for the bearings under high loads, vibration, low speeds and occasional oscillating motion [44].

The tests were performed with four fully formulated lubricants, with the same viscosity grade as all wind turbine gear oils, ISO VG 320. For that matter, a mineral (MINR), a polyalpholephin (PAOR), a hydro-processed group III mineral with polyalkyl methacrilate as viscosity index improver (MINE) and a polyalkylene glycol (PAGD) were studied.

The mentioned lubricants were also used in previous works with the same gearbox by Pereira [13] and Camacho [14], and their chemical compounds and physical properties are presented in table 4.1.

At a chemical level, PAGD is the lubricant that presents more differences towards the other oils. As it can be seen in table 4.1, the amount of phosphorus in its constitution is three times higher while the concentration of sulfur and boron is ten times lower in comparison to others. Phosphorus, boron and sulfur are known to be used in the chemical composition of the gear oils as extreme pressure additives.

The kinematic viscosity variation with temperature was studied applying Vogel's law given by equation (4.1).

$$\nu = K \exp\left(\frac{b_v}{\theta + c}\right) \tag{4.1}$$

At 40 °C the lubricants present similar viscosity, given the viscosity grade, except for PAGD, which is lower. On the range of temperature analyzed, MINR is the oil with the highest viscosity variation and PAGD the lowest which is reflected by the viscosity index, presented in table 4.1.

Density variation with temperature is calculated through equation (4.2).

Table 4.1: Lubricants chemical composition and physical properties.

| | | MINR | PAOR | MINE | PAGD |
|---|---|---|---|---|---|
| **Base oil:** | | Mineral | Poly$-\alpha-$olefin | Mineral +40% PAMA | Polyalkalene Glycol |
| **Chemical compounds** | | | | | |
| **Zinc (Zn)** | /ppm | 0.9 | <1 | 3.5 | 1.0 |
| **Magnesium (Mg)** | /ppm | 0.9 | <1 | 0.5 | 1.4 |
| **Phosphorus (P)** | /ppm | 354.3 | 460 | 415.9 | 1100 |
| **Calcium (Ca)** | /ppm | 2.5 | 2 | 0.5 | 0.8 |
| **Boron (B)** | /ppm | 22.3 | 36 | 38.4 | 1.0 |
| **Sulfur (S)** | /ppm | 11200 | 6750 | 5020 | 362 |
| **Physical Properties** | | | | | |
| **Density @ 15 °C** | /g/cm$^3$ | 0.902 | 0.859 | 0.893 | 1.059 |
| **Viscosity @ 40 °C** | /cSt | 319.25 | 324.38 | 324.38 | 290.26 |
| **Viscosity @ 70 °C** | /cSt | 65.87 | 87.92 | 97.72 | 102.33 |
| **Viscosity @ 100 °C** | /cSt | 22.41 | 35.27 | 37.88 | 51.06 |
| **Viscosity Index** | /- | 85 | 155 | 166 | 241 |
| **Thermoviscosity @ 40 °C** ($\beta_t \times 10^{-3}$) | /K$^{-1}$ | 63.88 | 50.68 | 49.33 | 37.34 |
| **Thermoviscosity @ 70 °C** ($\beta_t \times 10^{-3}$) | /K$^{-1}$ | 42.83 | 36.16 | 35.48 | 28.36 |
| **Thermoviscosity @ 100 °C** ($\beta_t \times 10^{-3}$) | /K$^{-1}$ | 30.07 | 26.72 | 26.40 | 22.12 |
| **Piezoviscosity @ 40 °C** ($\alpha_p \times 10^{-8}$) | /Pa$^{-1}$ | 2.207 | 1.590 | 1.600 | 1.278 |
| **Piezoviscosity @ 70 °C** ($\alpha_p \times 10^{-8}$) | /Pa$^{-1}$ | 1.774 | 1.339 | 1.353 | 1.105 |
| **Piezoviscosity @ 100 °C** ($\alpha_p \times 10^{-8}$) | /Pa$^{-1}$ | 1.527 | 1.182 | 1.197 | 0.988 |
| **Equations' parameters** | | | | | |
| **Thermal expansion coefficient** ($\alpha_k \times 10^{-4}$) | /K$^{-1}$ | -5.8 | -5.6 | -6.7 | -7.1 |
| **Constant** K | /cSt | 0.0815 | 0.1875 | 0.2033 | 1.5068 |
| **Constant** $b_v$ | /°C | 1051.8190 | 1043.2300 | 1072.4920 | 638.4920 |
| **Constant** c | /°C | 87.1290 | 100.5561 | 105.1729 | 81.3362 |

$$\rho = \rho_0 + \alpha_k \cdot \rho_0(\theta - 15) \tag{4.2}$$

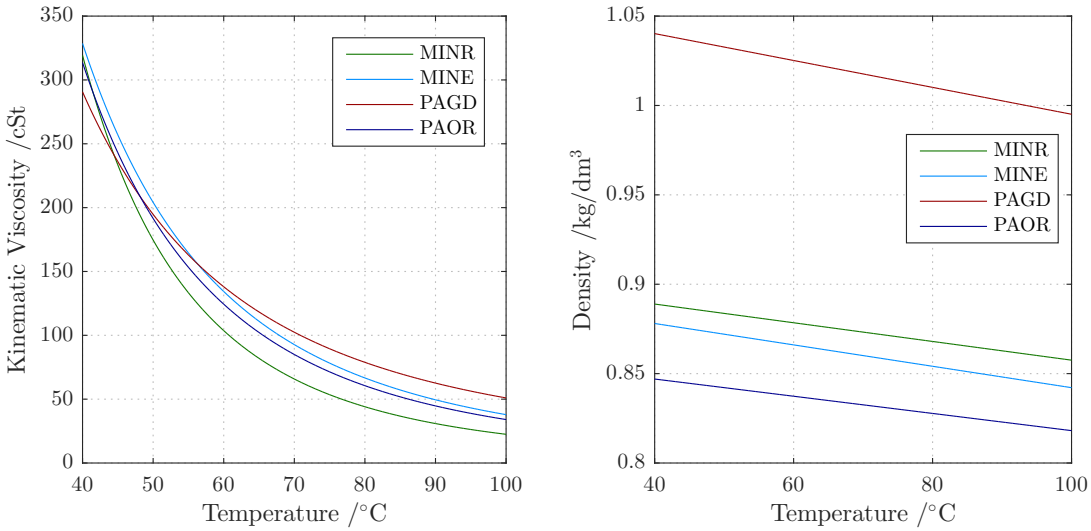


(a) Kinematic viscosity variation.

(b) Density variation.

Figure 4.1: Lubricants viscosity and density variation with temperature.

All oils show a linear decrease of density with increasing temperature. PAGD presents the steepest variation and a much higher density than the others lubricants while PAOR presents the lowest.

In table 4.1 are also presented the values of piezoviscosity and thermoviscosity that represent the oil viscosity behaviour with pressure and temperature, respectively.

## 4.2 Planetary Gearbox

### 4.2.1 General Description

The planetary configuration of the gearbox allows a compact design where both the input and output shafts are aligned. Planetary gearboxes also allow high transmission ratios and higher power transmission per unit of volume (power density). These characteristics make them very interesting for many applications, namely wind turbines transmission systems.

The planetary gearbox used in this work was a speed multiplier with a gear ratio of 4 and with nominal values of input speed and output torque of 1000 rpm and 2500 N·m, respectively. The specifications sheet of the gearbox is presented in Appendix A.

The tested gearbox was disassembled and details of the inside may be seen in figure 4.2.

In the present work the planetary gearbox was tested on a reducer configuration. This allowed the utilization of a smaller capacity motor in the test rig.

After the gearbox being disassembled, the gears were measured and their characteristics are presented in table 4.2


Figure 4.2: Tested planetary gearbox disassembled.

Table 4.2: Geometrical characteristics of the gears in the planetary gearbox.

| | | **Sun** | **Planet** | **Ring** |
|---|---|---|---|---|
| $m$ | /mm | | 2 | |
| $\alpha$ | /° | | 20 | |
| $\beta$ | /° | | 11 | |
| $z_i$ | /- | 36 | 36 | -108 |
| $b$ | /mm | 42 | 40 | 42 |
| $x$ | /- | $-0.0536$ | $-0.0536$ | 0.1609 |
| $k$ | /- | $-0.0665$ | $-0.0665$ | 0 |
| $Ra$ | /$\mu$m | | 0.08 | |
| $D_p$ | /mm | 73.348 | 73.348 | -220.043 |
| $D_b$ | /mm | 68.772 | 68.772 | -206.318 |
| $D_a$ | /mm | 77.000 | 77.000 | -215.399 |
| $D_w$ | /mm | 73.131 | 73.131 | -219.392 |
| $\alpha_{tw}$ | /° | | 19.880 | |
| $a$ | /mm | | 73.348 | |
| $a_w$ | /mm | | 73.131 | |

In table 4.3 the number and reference of bearings and shaft seals are presented. Both needle and tapered roller bearings were lubricated with gear oil while the deep groove ball bearing was shielded, so it was lubricated with grease (figure 4.3c).

Table 4.3: Bearings and seals in the planetary gearbox.

| Component | Quantity | Reference |
|---|---|---|
| **Tapered roller bearing (TRB)** | 2 | 32022 X/Q |
| **Deep groove ball bearing (DGB)** | 1 | 6217-2Z |
| **Input seal (lip seal)** | 1 | BAUM6 SLX7 140×170×13 |
| **Output seal (lip seal)** | 1 | 72×100×10 |
| **Full-complement needle roller bearing (NRB)** | 3 sets of 23 needle rollers | 6×23 |

In figure 4.3 other details of the gearbox interior are shown. For instance, in figure 4.3a it's possible to see that the planet carrier is part of a machined shaft. Other curious aspect, in figure 4.3b, is that the needle roller bearings are located between the sleeve and the planet gear without cage, called full-complement needle roller bearings. This is a good solution when one looks for a compact design. However, it may be quite inefficient due to the roller-roller sliding.

(a) Planet carrier. (b) Planet gear with the full-complement needle roller bearings. (c) Sun gear.

Figure 4.3: Details of the planetary gearbox.

### 4.2.2 Kinematic Analysis

The power loss of all the components in the gearbox is dependent of the speed at which they operate. Therefore, a kinematic analysis is done in order to determine the speeds involved [14]. The ring gear is fixed.

A schematic representation of the main components of the gearbox it is shown in figure 4.4, where:

1. Sun gear.
2. Planet Gear
3. Ring gear.
4. Planet carrier.

The absolute speeds of the referred components are related through the following equations [14].

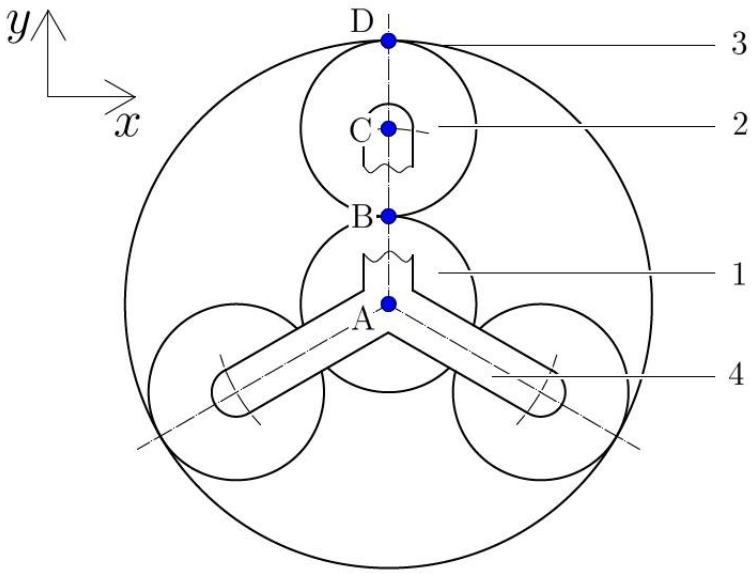


Figure 4.4: Schematic representation of the planetary gear [14].

$$\omega_{10} = \omega_{40} \cdot 2 \cdot \left(1 + \frac{z_2}{z_1}\right) = \omega_{40} \cdot (1 + \frac{z_3}{z_1}\Big) \tag{4.1}$$

$$\omega_{20} = -\omega_{40} \cdot \left(1 + \frac{z_1}{z_2}\right) \tag{4.2}$$

The gear ratio, $u$, of the gearbox is function exclusively of the number of teeth of each gear and it is given by:

$$u = 1 + \frac{z_3}{z_1} \tag{4.3}$$

Or,

$$u = 2 + \frac{2 \cdot z_2}{z_1} \tag{4.4}$$

Substituting the values presented in table 4.2 in equation (4.3) for the ring and sun gears the gear ratio comes as 4, as referred before. As the gearbox is in a reducer configuration the power input will be made by the sun gear, while the power output is made by the planet carrier, with a quarter of the speed.

Following the gear ratio, the planet carrier speed, $\omega_{40}$, is calculated according to equation (4.5). This speed is the one at which the tapered roller bearings are submitted, since they are located in the output shaft.

$$\omega_{40} = \frac{\omega_{10}}{u} \tag{4.5}$$

To find the speed of the sun gear relative to a referential attached to the planet carrier, $\omega_{14}$, the speed of the planet carrier, calculated in equation (4.5), must be subtracted to the absolute speed of the sun gear, as presented in equation in equation (4.6).

$$\omega_{14} = \omega_{10} - \omega_{40} \tag{4.6}$$

The speed of the planet gear relative to a referential that runs attached to the planet carrier, $\omega_{24}$, is calculated with equation (4.7). This speed is important when considering the power loss in full-complement needle roller bearings. Since a referential rotating attached to the planet carrier is considered, the centers of the planets remain stationary according to this referential.

$$\omega_{24} = -\omega_{14} \cdot \frac{z_1}{z_2} \tag{4.7}$$

As $z_1 = z_2$, the relative speed is the same for the sun and planet gears.

The relative speed of the ring gear, $\omega_{34}$, is equal (in absolute value) to the speed of the planet carrier.

$$\omega_{34} = -\omega_{40} \tag{4.8}$$

## 4.3 No-Load Gearbox Test Rig (NLGTR)

The test rig used to measure the no-load torque loss is shown in figure 4.5. The multiplier gearbox was assembled in 'speed reducer' configuration for the purpose of these measurements.

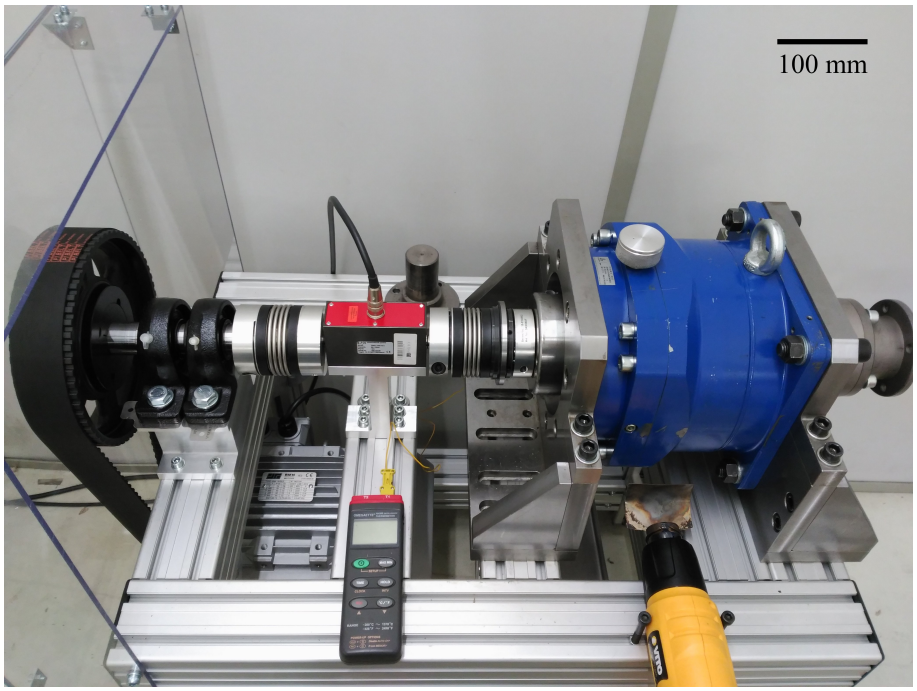


Figure 4.5: Test rig.

The rotation speed at which each test was conducted was referred to the output shaft. So, as the tested gearbox presents a gear ratio of 4 and the belt and pulley system a ratio of 3, the speed of the electrical motor was 12 times greater than the output speed. This allowed

a more efficient control of the motor. The speed was set in the control dashboard, shown in figure 4.6a.

The electric motor used has a nominal power of 7.5 kW, a maximum rotation speed of 2920 rpm and nominal values of tension and frequency of 400 V and 50 Hz, respectively.

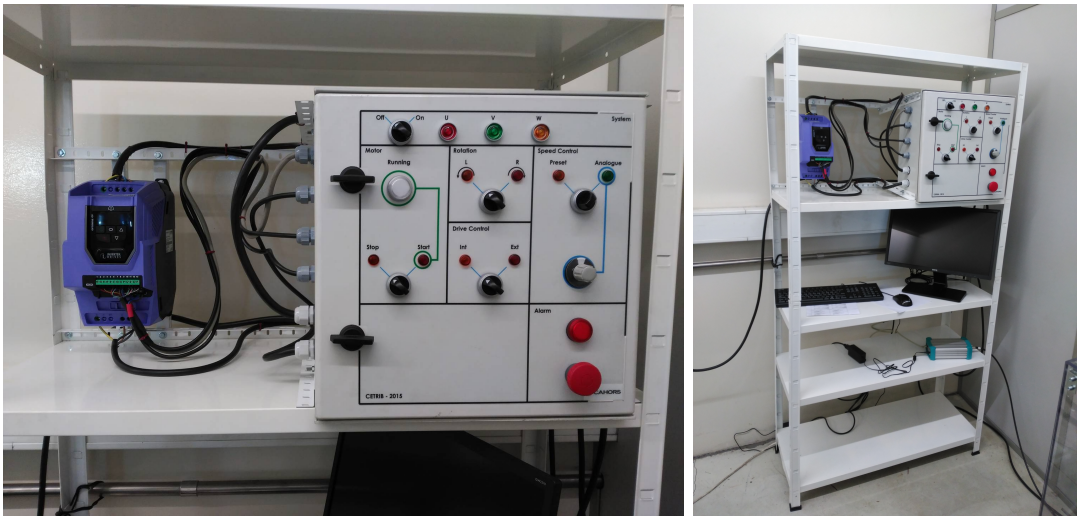

(a) Control dashboard of the NLGTR. (b) Central Control

Figure 4.6: Central Control of the NLGTR.

The torque transducer located between the input of the planetary gearbox and the pulley, was connected to a computer, presented in figure 4.6b, through an acquisition data system which allowed recording the torque results for each test. In table 4.4 the specifications of the torque cell and data acquisition device are presented.

Table 4.4: Technical specifications of the ETH DRDL II torque cell.

| Torque Transducer Type DRDL | | |
|---|---|---|
| **Nominal torque** | /N·m | 50 |
| **Measurement range** | /N·m | 5/10/20/50 |
| **Non-linearity** | /% | $< 0.1$ |
| **Hysteresis** | /% | $< 0.1$ |
| **Accuracy** | /% | 0.01 |
| **Temperature sensitivity** | /%/K | 0.01 |
| Torque Measuring Module Type *Value Master*$_{Base}$ | | |
| **Accuracy** | /% | 0.02 |
| **Non-linearity** | /% | 0.1 |
| **AD converter resolution** | /- | 11 bit + 1 bit for leading sign |

The oil temperature inside the gearbox was measured through a sensor, a type K thermocouple that was connected to a data logger, OMEGAETTE HH306 THERMOMETER, which had the possibility of recording temperature data when necessary. Both are shown in detail in figure 4.7. The heat gun, seen in figure 4.5, was used for a forced oil heating.


(a) Temperature sensor. (b) Data Logger.

Figure 4.7: Details of the temperature measurement on the test rig.

## 4.4 Complement of Previous Load Tests

In previous works [14], the operating conditions of the gearbox were similar to those imposed to the first stage of a 2.5 MW wind turbine gearbox in terms of tangential speed and Hertzian pressure. The tangential speed, dependent on the rotation speed, and the Hertzian pressure, dependent on the torque, were calculated with *KISSsoft* software [14], and are presented in table 4.5.

Table 4.5: Tangential speed and Hertzian pressure in a 2.5 MW wind turbine [14].

| **Gear Stage** | **Tangential Speed** m/s | **Hertz Pressure** $N/mm^2$ |
|---|---|---|
| $1^{st}$ Stage | 1.63 | 1382 (SP) |
| | | 988 (PR) |
| $2^{nd}$ Stage | 5.49 | 2873 (SP) |
| | | 2029 (PR) |

SP – Sun-Planet contact

PR – Planet-Ring contact

In this work, the conditions imposed to the test gearbox were controlled in terms of the output shaft rotation speed. Since the experiments were performed under no-load conditions, the torque measurements were made at the stabilization temperatures measured on the experimental campaign realized by Camacho [14], where the goal was to evaluate the influence of operating conditions and gear oil formulation in the planetary gearbox. Table 4.6 presents the operating conditions used by Camacho [14].

Table 4.6: Tangential speed and Hertzian pressure in the tested gearbox on Camacho's tests [14].

| **Imposed rotational speed** rpm | **Tangential speed** m/s | **Imposed torque** N·m | **Hertz pressure** N/mm$^2$ |
|---|---|---|---|
| 100 | 1.15 | 2000 | 1064 (SP) |
| | | | 720 (PR) |
| 150 | 1.72 | 2400 | 1165 (SP) |
| | | | 786 (PR) |
| 200 | 2.30 | 2800 | 1249 (SP) |
| | | | 846 (PR) |

## 4.5 Test Planning

### 4.5.1 Single Tests

Firstly, a set of single tests, with an oil volume of 1 litre, were made to complement the results of the work made by Camacho [14] with an accurate prediction of the churning power loss after numerical treatment. To provide a more complete information, the measurements were also made with an oil volume of 0.75 litre. Every test was repeated for each rotation direction, S1 and S2. The planning is presented in table 4.7

Table 4.7: Single tests planning.

| **Oil** | $V_m$ L | $n$ rpm | $M_{load}$ N·m |
|---|---|---|---|
| MINR/PAOR/MINE/PAGD | 0.75/1 | 100 | 2800 |
| | | 150 | 2000 |
| | | | 2400 |
| | | | 2800 |
| | | 200 | 2800 |

The temperature at which torque measurements were made are presented in table 4.8 for MINR and in tables 4.9, 4.10 and 4.11 for PAOR, MINE and PAGD respectively. Despite the presented temperatures measured by Camacho [14] correspond to the stabilization temperatures concerning one litre of lubricant, the experiments were conducted equally with 0.75 litre with the purpose of comparison between two different volumes.

Table 4.8: Target temperatures, in °C, for torque measurements with MINR.

| Oil: | MINR | | |
|---|---|---|---|
| | $M_{load}$ /N·m | | |
| $n$ /rpm | 2000 | 2400 | 2800 |
| 100 | - | - | 60.26 |
| 150 | 68.50 | 70.66 | 73.36 |
| 200 | - | - | 84.50 |

Table 4.9: Target temperatures, in °C, for torque measurements with PAOR.

| Oil: | PAOR | | |
|---|---|---|---|
| | $M_{load}$ /N·m | | |
| $n$ /rpm | 2000 | 2400 | 2800 |
| 100 | - | - | 55.32 |
| 150 | 62.86 | 65.08 | 68.84 |
| 200 | - | - | 78.03 |

Table 4.10: Target temperatures, in °C, for torque measurements with MINE.

| Oil: | MINE | | |
|---|---|---|---|
| | $M_{load}$ /N·m | | |
| $n$ /rpm | 2000 | 2400 | 2800 |
| 100 | - | - | 55.13 |
| 150 | 62.85 | 64.72 | 66.34 |
| 200 | - | - | 73.72 |

Table 4.11: Target temperatures, in °C, for torque measurements with PAGD.

| Oil: | PAGD | | |
|---|---|---|---|
| | $M_{load}$ /N·m | | |
| $n$ /rpm | 2000 | 2400 | 2800 |
| 100 | - | - | 57.05 |
| 150 | 65.54 | 68.19 | 70.01 |
| 200 | - | - | 80.33 |

### 4.5.2 Continuous Tests

For the second set of tests, described in table 4.12, the behaviour of the oils in terms of the evolution of no-load losses was measured under different conditions. This then allowed to study the churning phenomenon in a planetary gearbox. These tests were also made for both directions, S1 and S2.

Table 4.12: Continuous tests planning.

| **Oil** | $V_m$ L | $n$ rpm |
|---|---|---|
| MINR/PAOR/MINE/PAGD | 0.75/1 | 100 |
| | | 200 |

## 4.6 Experimental Procedure

In the beginning of every experiment the gearbox was filled with 0.75 or 1 litre of fresh lubricant through a plug hole in the top, seen in figure 4.8a. The rotation speed of the output shaft was set in the control central, knowing that the speed of the motor was 12 times higher as it was previously explained. The heat gun was always on for oil heating and the temperature data logger was used for temperature measurement.

For the single tests, the torque measurements were taken in the target temperature presented in chapter 4.5 for each oil, starting at the lowest rotation speed and ending on the highest. As the torque cell presented some oscillation around the value that was truly being measured, the measurement started 1 °C below the target temperature and was stopped 1 °C above. This was done with an acquisition data software, *Value Master*, whose interface is shown in figure 4.8b. Then, the average value was considered.

For continuous tests, the speed was set in the control central and the temperature was recorded through the data logger for numerical treatment.

In the end of each experiment, the oil was drained through a plug hole in the bottom and then the gearbox was filled with petroleum ether, except for PAGD which was flushed with a special solvent, a mix of propanol and tuolene. While the gearboxes were filled with solvent, the gearbox shaft was set to a low speed for several minutes aiming to remove the maximum amount of remaining oil and wear particles. Then, the solvent was removed the same way as the oil. Usually, the next oil to be tested was only inserted the next day, in order to let the remaining solvent evaporate.

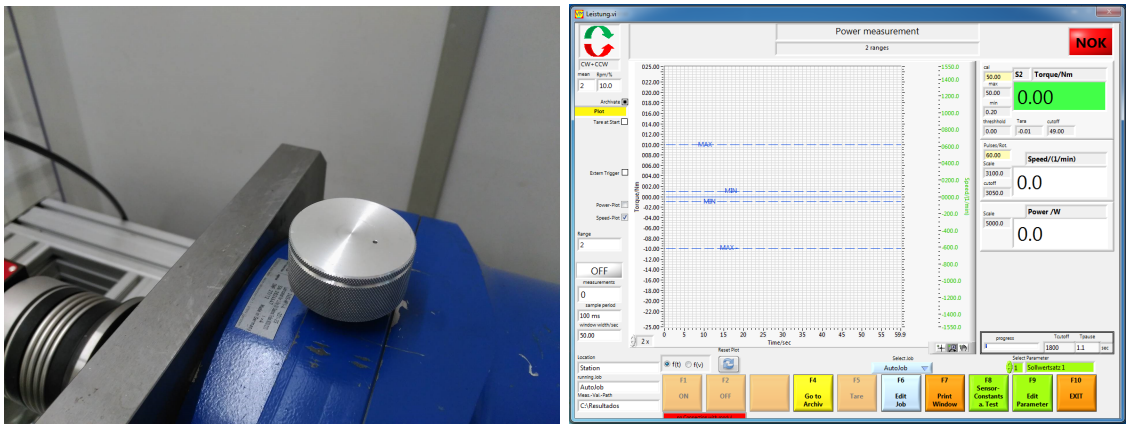


(a) Top plug hole. (b) *Value Master* interface.

Figure 4.8: Top plug hole and *Value Master* interface.

# CHAPTER 5

# No-Load Loss

In this chapter, the no-load losses are discussed. The measurements for each oil are presented for two different volumes and rotation directions, S1 and S2. Each test was repeated twice and the results are presented in Appendix B to demonstrate the consistency of the measured values and then the average between them was considered. Then, one tries to understand the sources of power dissipation by breaking down the different power loss sources according to equation 5.1. For this analysis the average value between directions S1 and S2 was considered. In order to account for the different rotation speeds of the different components the no-load losses are presented and decomposed in terms of power loss instead of torque loss. Each one of the no-load power loss components, except churning, were calculated by the models presented in Chapter 3.

$$P_V = P_{VZ0} + P_{VX} + P_{VL0} + P_{VD} \tag{5.1}$$

To consider the churning power loss, $P_{VZ0}+P_{VX}$, one has to proceed according to equation (5.2), knowing that $P_V^{exp}$ is the measured value of power loss and the other components are calculated as referred above.

$$P_{VZ0} + P_{VX} = P_V^{exp} - (P_{VL0} + P_{VD}) \tag{5.2}$$

Where the bearings no-load power loss is calculated through equation (5.3).

$$P_{VL0} = P_{VL0}^{FCNRB} + P_{VL0}^{TRB} \tag{5.3}$$

Finally, a comparison between all gear oils used is made and the differences presented are explained.

## 5.1 MINR

The no-load torque measurements for constant load torque and constant speed are shown in figures 5.1 and 5.2, respectively. It can be seen that the results don't present any significant difference for the two volumes used.

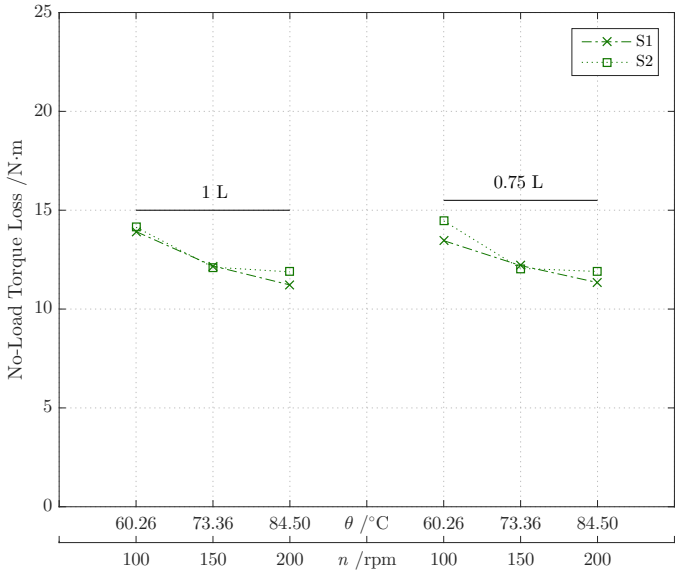


Figure 5.1: No-load torque loss for MINR at the target temperatures of table 4.8.

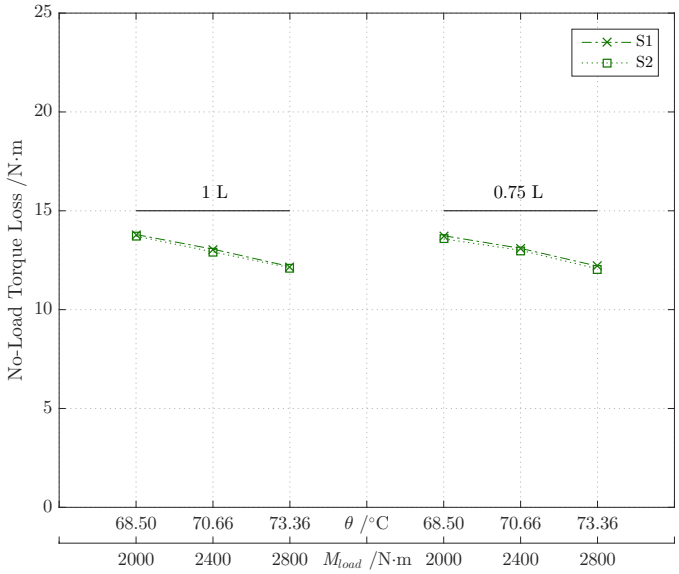


Figure 5.2: No-load torque loss for MINR at the target temperatures of table 4.8.

The measurements for constant speed reveal a great consistency, showing very similar results for both S1 and S2.

In figures 5.3a and 5.3b the no-load power loss is divided in its components. The power loss produced by tapered roller bearings ($P_{VL0}^{TRB}$) are very relevant and are strongly dependent on the rotation speed, as expected.

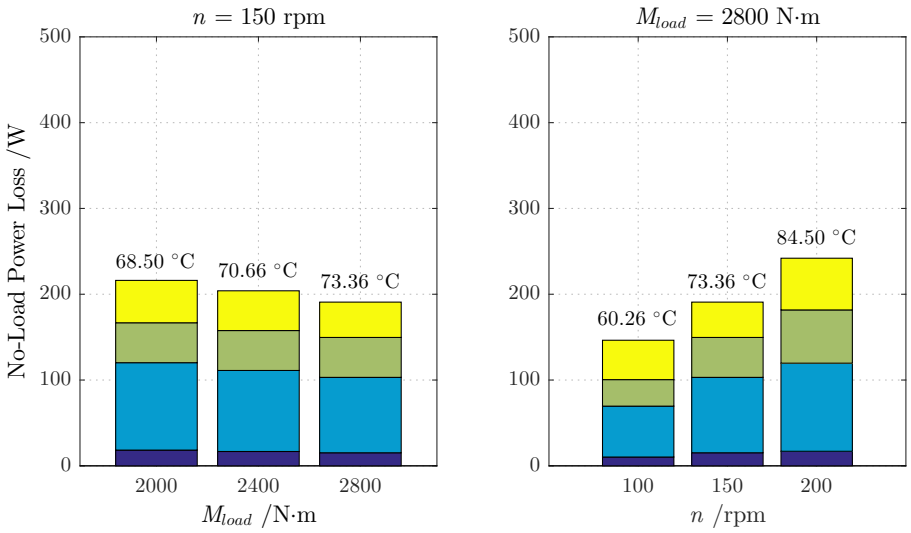


(a) $V_m$ = 1 L.

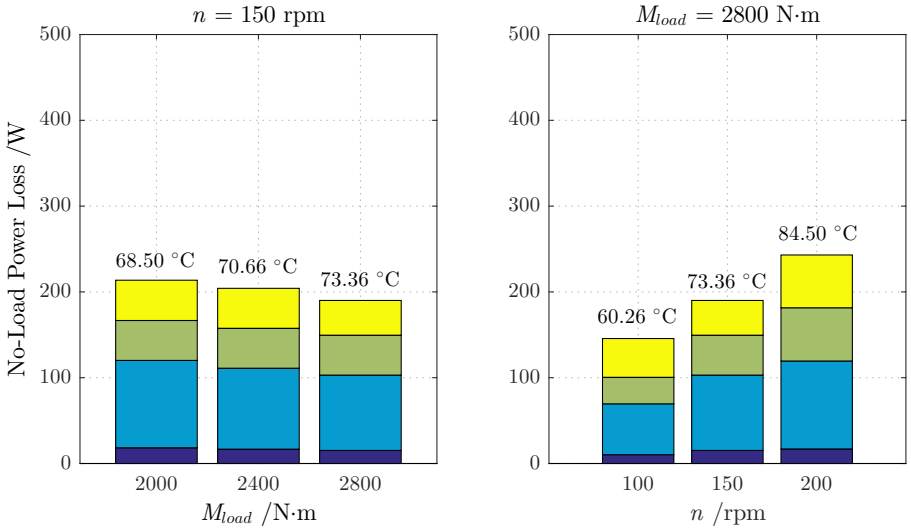


(b) $V_m$ = 0.75 L.

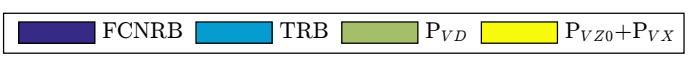


Figure 5.3: No-load power loss (numerical) for MINR divided in its different components at the target temperatures of table 4.8.

## 5.2 PAOR

For PAOR, the measurements presented in figures 5.4 and 5.5 are slightly different for the two volumes used, being lower for 0.75 litre. In terms of consistency, it follows the same trend as the one presented for MINR, with the measurements made for constant speed

showing practically no differences for S1 and S2.

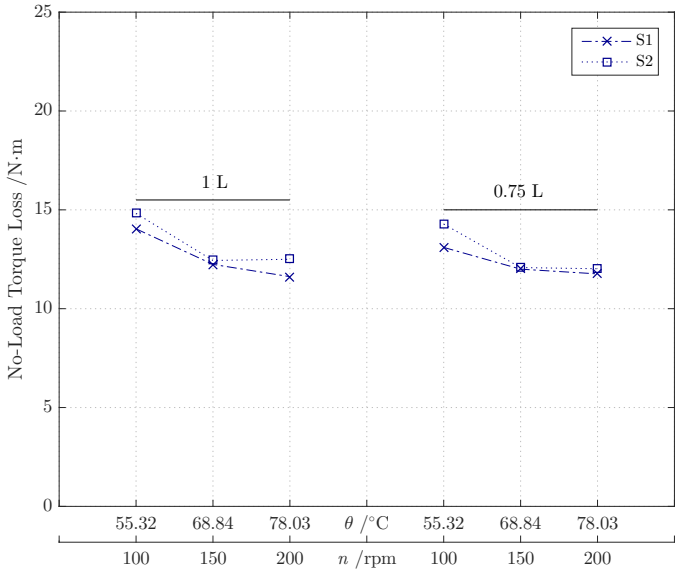


Figure 5.4: No-load torque loss for PAOR at the target temperatures of table 4.9.

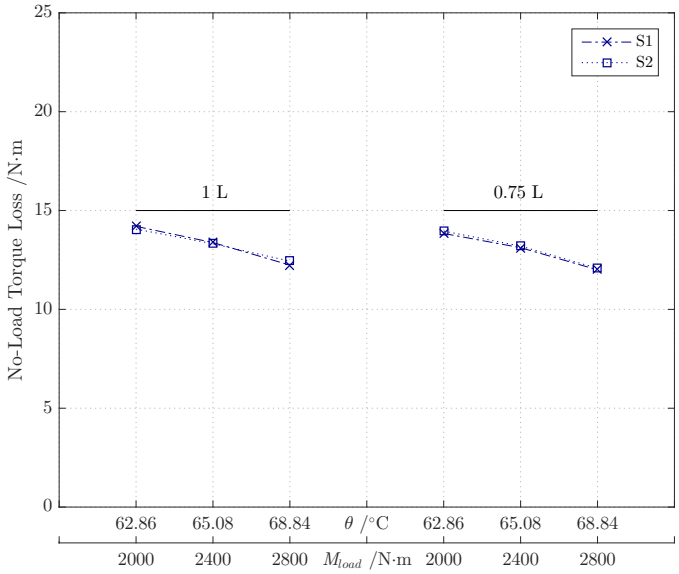


Figure 5.5: No-load torque loss for PAOR at the target temperatures of table 4.9.

In figures 5.6a and 5.6b one can see the lower influence of churning losses for a smaller oil volume.

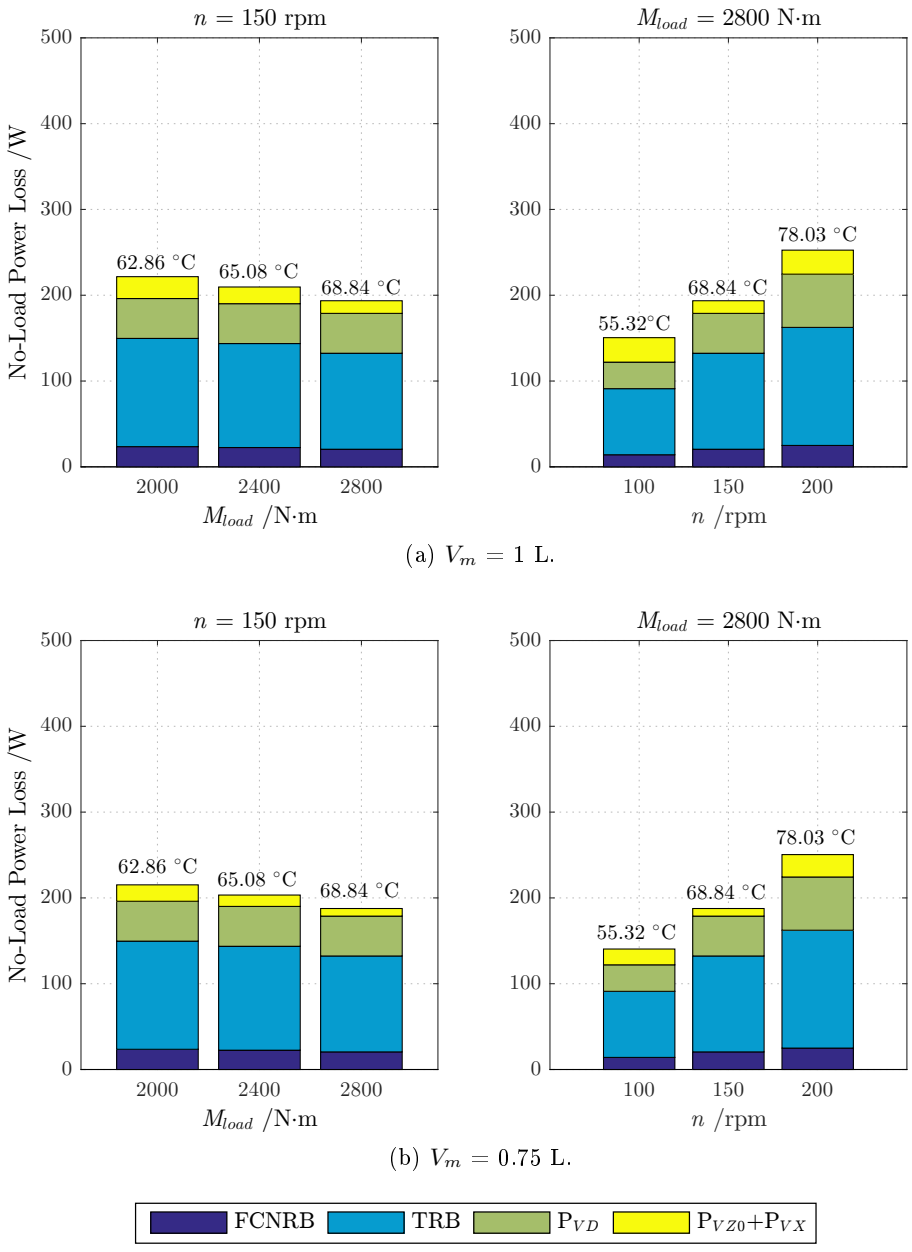


Figure 5.6: No-load power loss (numerical) for PAOR divided in its different components at the target temperatures of table 4.9.

## 5.3 MINE

MINE presents some differences toward the two gear oils referred before. For the same working condition, the no-load losses are slightly higher for the smaller oil volume with the churning losses presenting a more important role, as it may be seen in figures 5.9a and 5.9b.

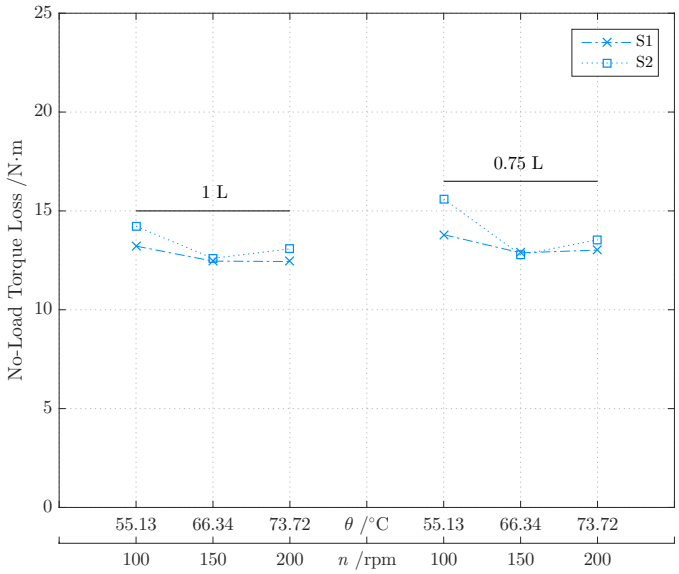


Figure 5.7: No-load torque loss for MINE at the target temperatures of table 4.10.

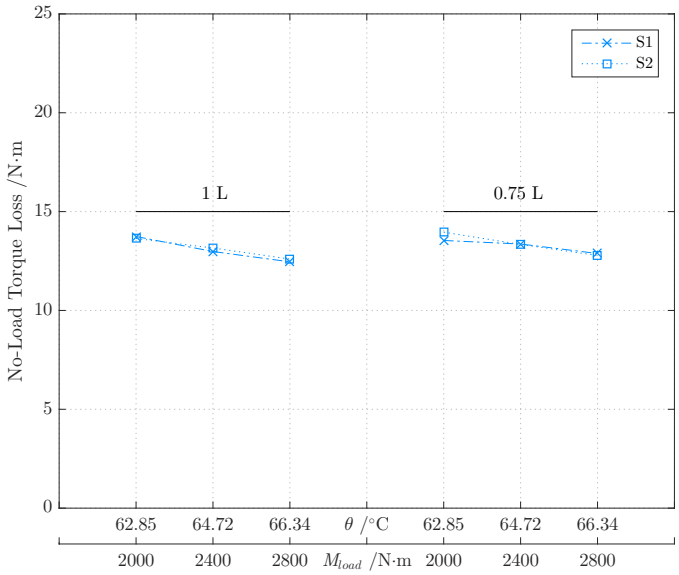


Figure 5.8: No-load torque loss for MINE at the target temperatures of table 4.10.

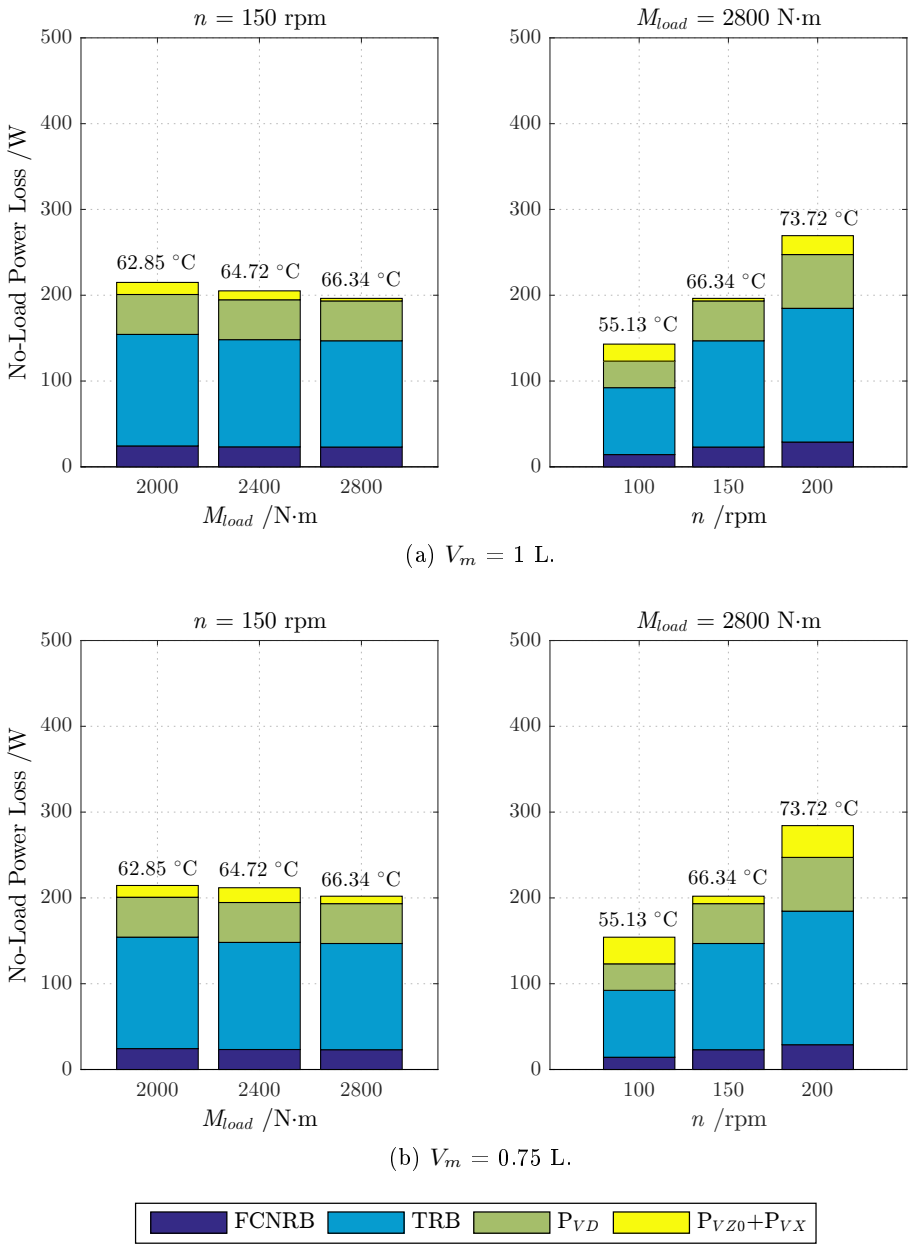


(a) $V_m$ = 1 L.

(b) $V_m$ = 0.75 L.

Figure 5.9: No-load power loss (numerical) for MINE divided in its different components at the target temperatures of table 4.10.

## 5.4 PAGD

The last lubricant to be tested, PAGD, showed a greater dependence on the oil volume. In figures 5.10 and 5.10 it's possible to see that for homologous points the no-load losses are quite more important when one uses 1 litre of gear oil.

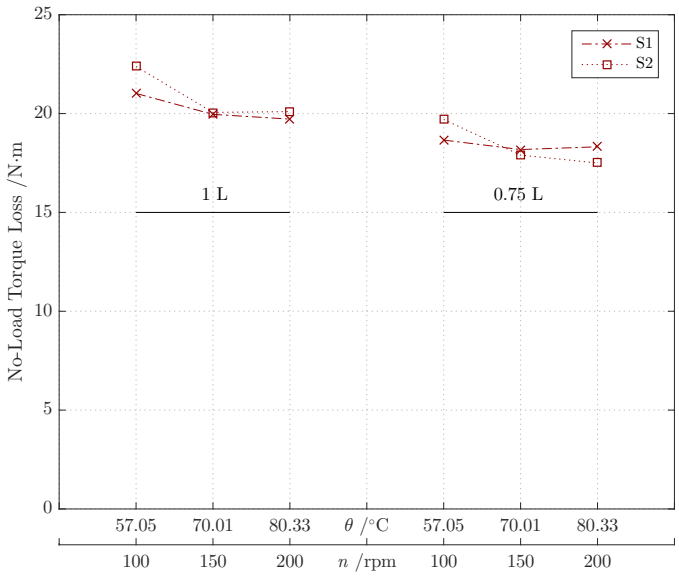


Figure 5.10: No-load torque loss for PAGD at the target temperatures of table 4.11.

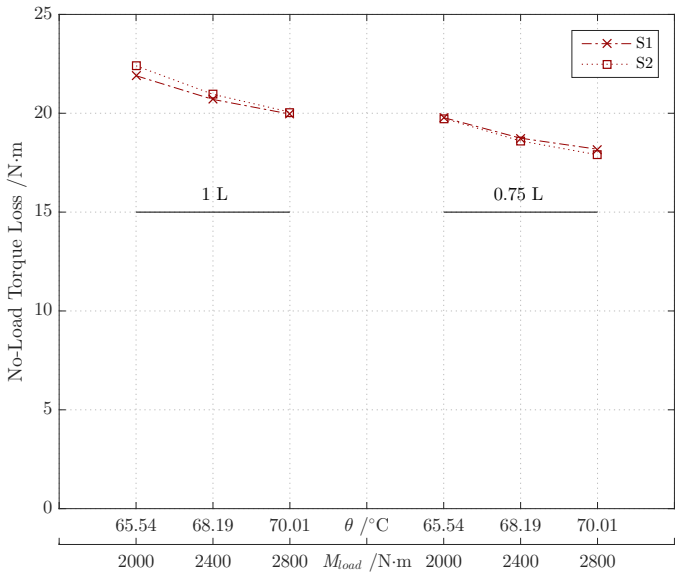


Figure 5.11: No-load torque loss for PAGD at the target temperatures of table 4.11.

With figures 5.12a and 5.12b it's possible to understand that the differences are produced mainly by churning power loss.

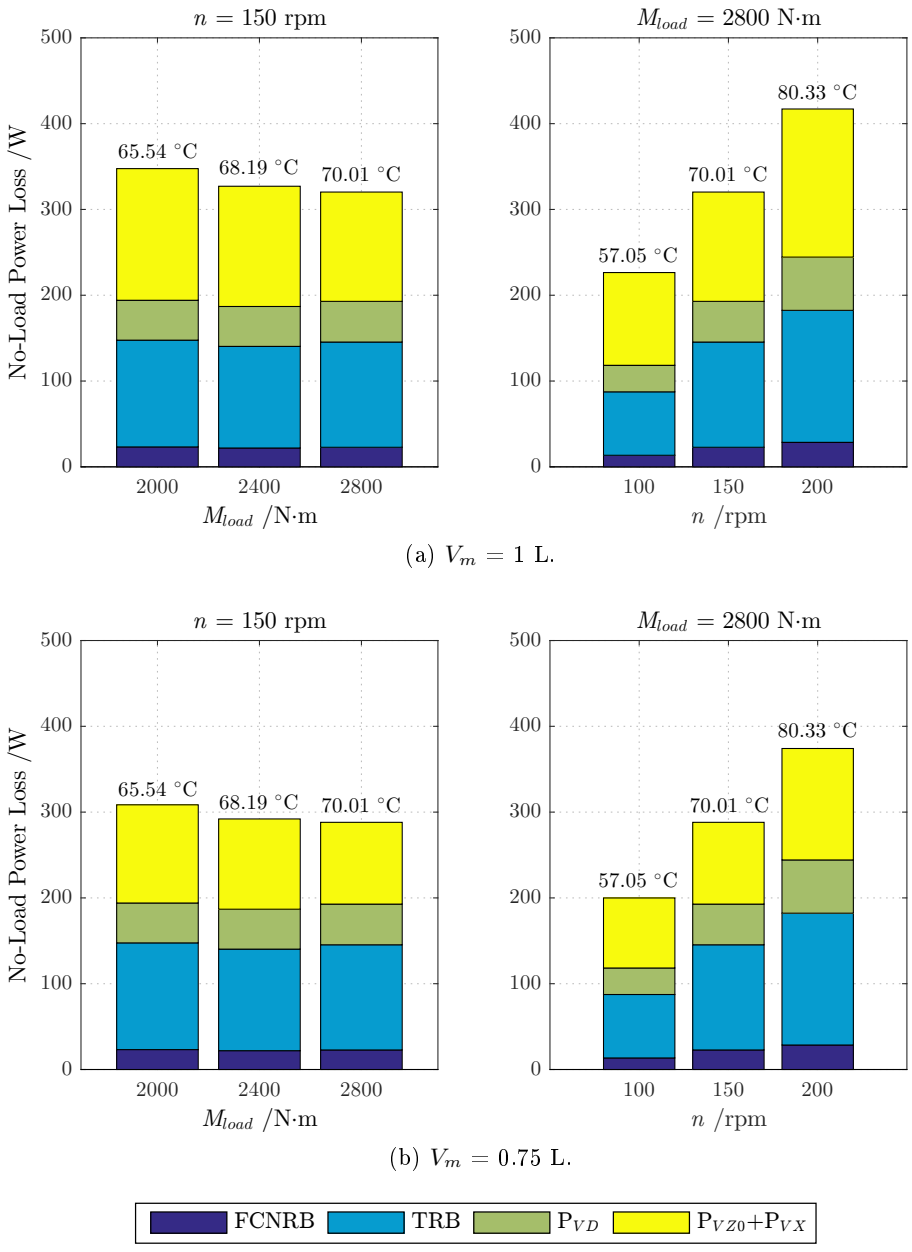


(a) $V_m$ = 1 L.

(b) $V_m$ = 0.75 L.

Figure 5.12: No-load power loss (numerical) for PAGD divided in its different components at the target temperatures of table 4.11.

## 5.5 Oils Comparison

In figures 5.13 and 5.14 the oils were compared in terms of no-load losses considering the average value between directions S1 and S2. Relative to each other the gear oils express the same type of behavior but in absolute values, PAGD presents much higher losses. The characteristic that may help to explain this difference, it's density, much higher for this oil as it was presented in chapter 4.1. So, with a higher oil mass to be accelerated the power loss becomes more important. For a constant load condition, MINE presents a slightly higher value than PAOR and MINR when one considers an oil volume of 0.75 litre.

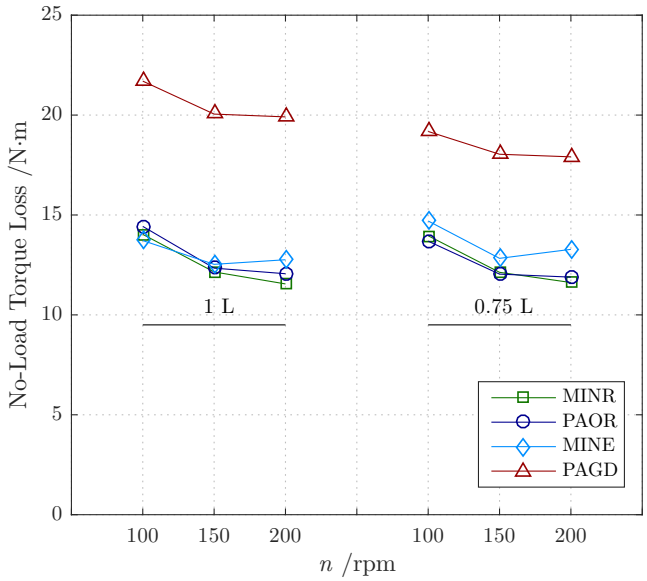


Figure 5.13: Oils comparison in terms of no-load torque loss at each oil target temperatures @ $M_{load}$ = 2800 N·m.

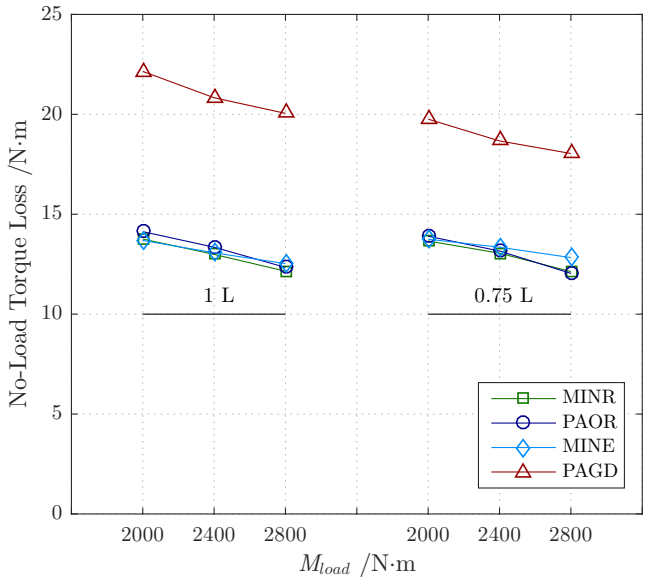


Figure 5.14: Oils comparison in terms of no-load torque loss at each oil target temperatures @ $n$ = 150 rpm.

The values of no-load power loss divided by each component are also presented under a tabular form in table 5.1.

Table 5.1: No-load power loss divided in its different components for $M_{load}$ = 2800 N·m and $n$ = 150 rpm.

| | **No-Load Power Loss** /W | | | | **No-Load Power Loss** /% | | | |
|---|---|---|---|---|---|---|---|---|
| **Oil (1 L)** | MINR | PAOR | MINE | PAGD | MINR | PAOR | MINE | PAGD |
| $P_{VL0}^{FCNRB}$ | 15.24 | 20.52 | 23.08 | 22.80 | 7.99 | 10.60 | 11.75 | 7.11 |
| $P_{VL0}^{TRB}$ | 87.88 | 111.90 | 123.90 | 122.70 | 46.05 | 57.79 | 63.09 | 38.31 |
| $P_{VD}$ | 46.52 | 46.47 | 46.45 | 47.41 | 24.38 | 24.00 | 23.65 | 14.80 |
| $P_{VZ0}$+$P_{VX}$ | 41.19 | 14.73 | 2.96 | 127.40 | 21.58 | 7.61 | 1.51 | 39.78 |
| **Total** | 190.83 | 193.62 | 196.39 | 320.31 | 100 | 100 | 100 | 100 |

# CHAPTER 6

# Churning Power Loss

The continuous tests allowed to study churning losses. Using equation (6.1), the churning power losses were calculated for each oil. As the results presented in chapter 5 showed a high consistency for both directions, when a constant speed was considered, the results presented in this chapter were considered only for direction S1. The values are presented for a range of Reynolds number of $500 < \text{Re} < 1600$. The Reynolds number considered is presented in equation (6.2) considering the pitch line speed, $v_t$, and pitch diameter, $D_p$, is referred to the sun gear presented in detail in table 4.2.

$$P_{VZ0} + P_{VX} = P_V^{exp} - (P_{VL0} + P_{VD}) \tag{6.1}$$

$$Re = \frac{v_t D_p}{\nu} \tag{6.2}$$

For every gear oil, the churning power loss decrease with the increase of the Reynolds number, with a trend similar to the one presented by kinematic viscosity variation with temperature. The differences with the oil volume are not very important, exception been made for PAGD, as one may see for the following figures. For a rotation speed of 200 rpm the discrepancy of values is much higher than for 100 rpm.

## 6.1 MINR

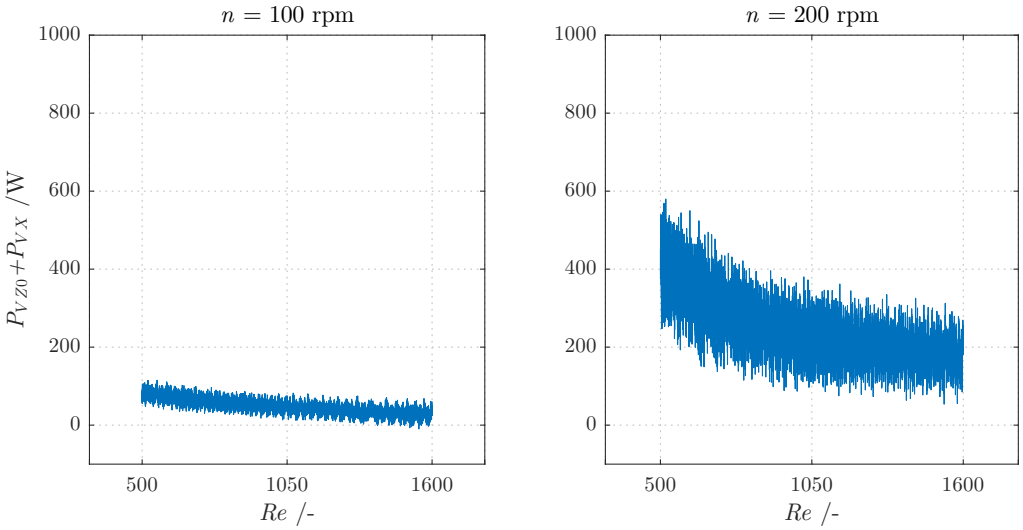


(a) $V_m = 1$ L.

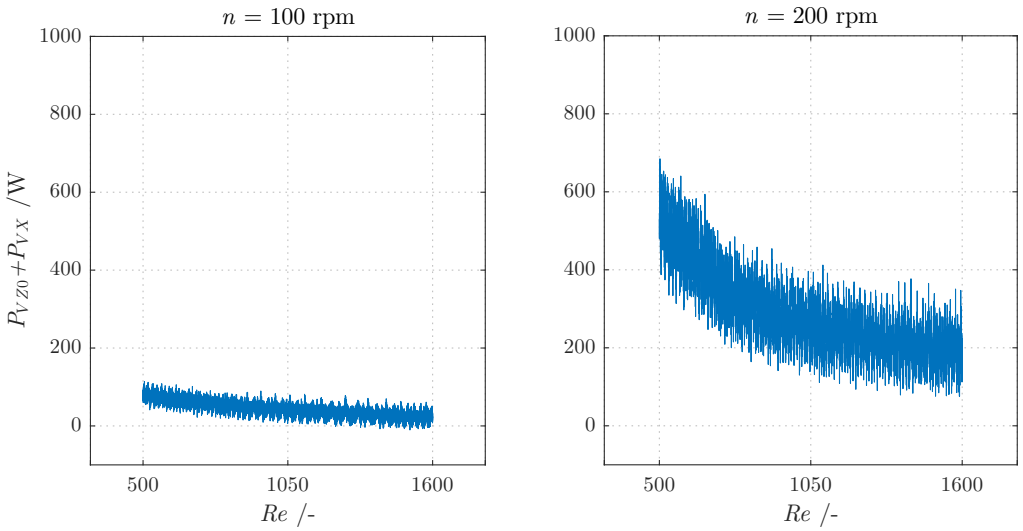


(b) $V_m = 0.75$ L.

Figure 6.1: Churning power loss for MINR.

## 6.2 PAOR

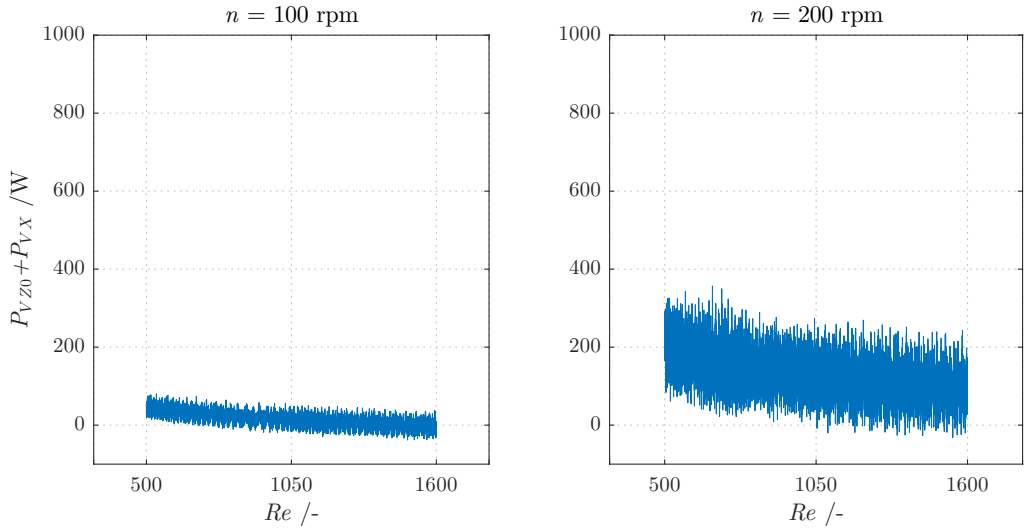


(a) $V_m = 1$ L.

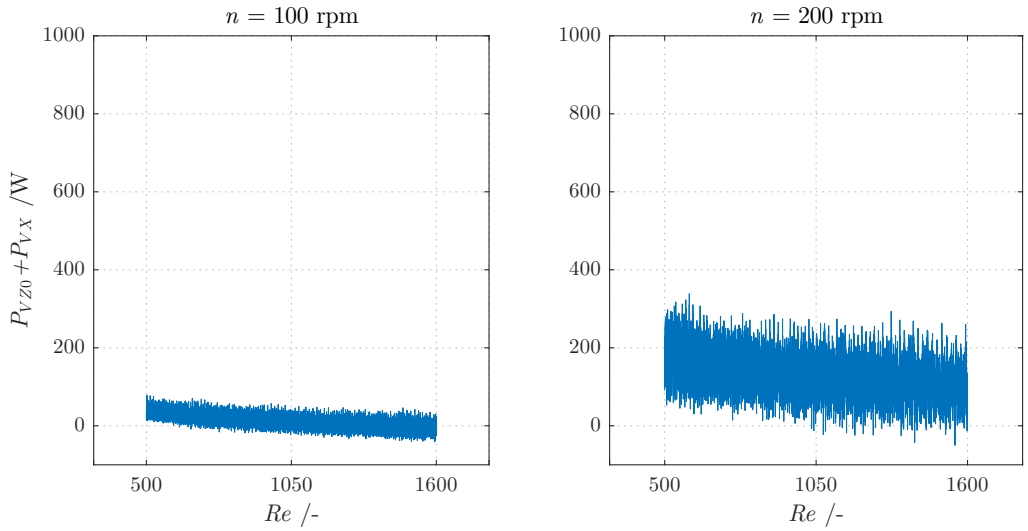


(b) $V_m = 0.75$ L.

Figure 6.2: Churning power loss for PAOR.

## 6.3 MINE

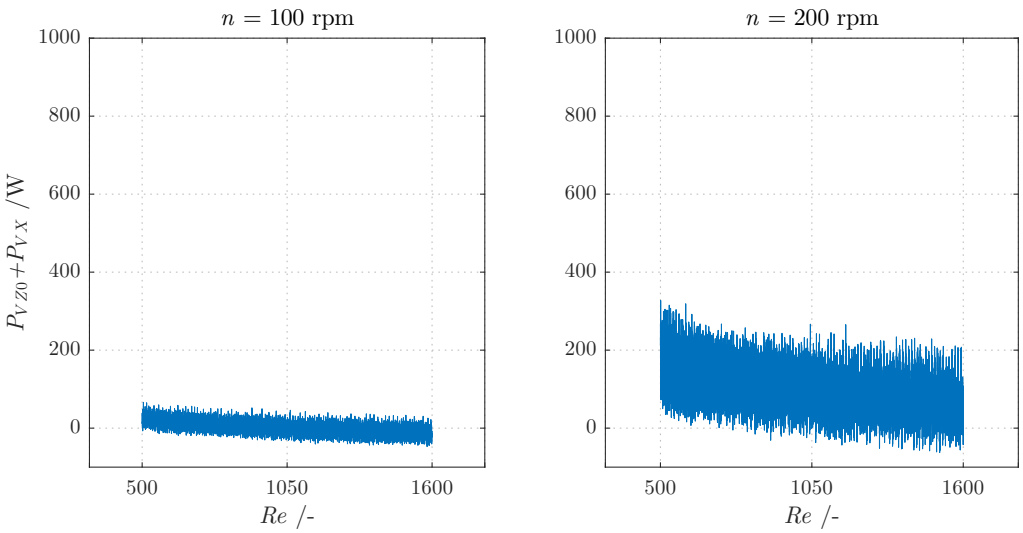


(a) $V_m = 1$ L.

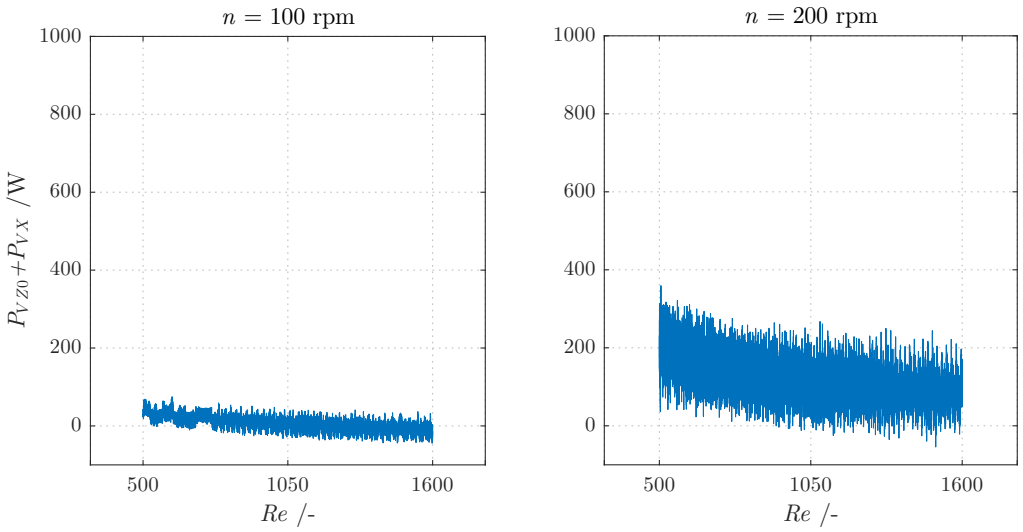


(b) $V_m = 0.75$ L.

Figure 6.3: Churning power loss for MINE.

## 6.4 PAGD

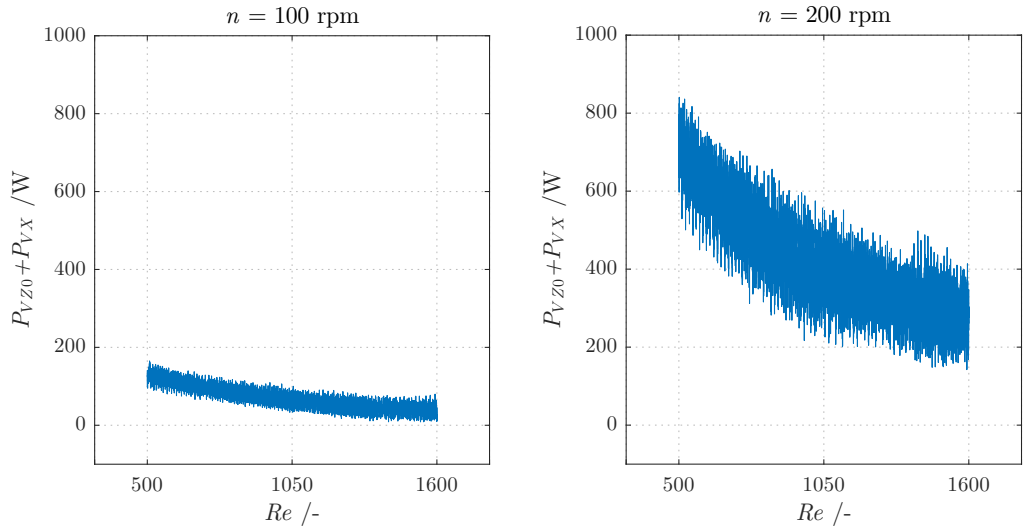


(a) $V_m = 1$ L.

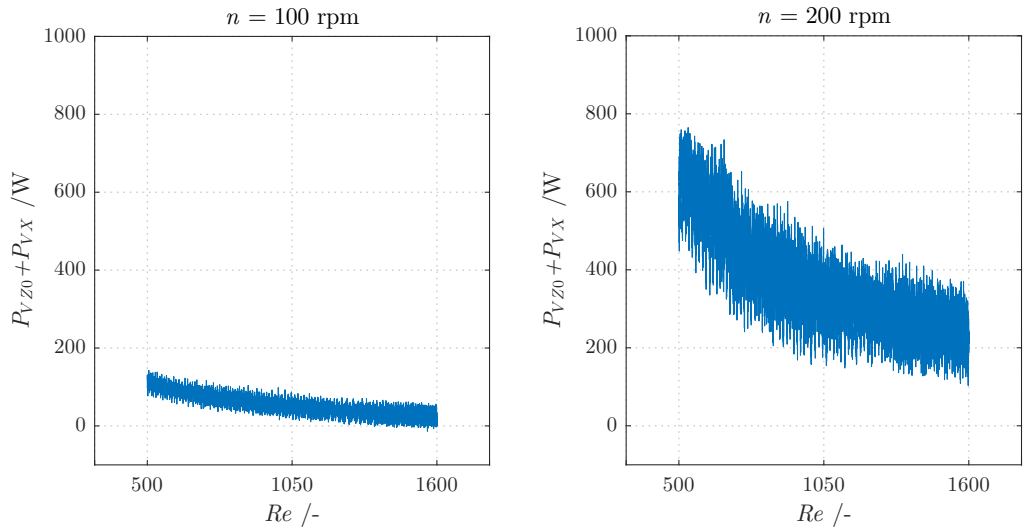


(b) $V_m = 0.75$ L.

Figure 6.4: Churning power loss for PAGD.

# CHAPTER 7

# Global Power Loss

Finally, the results of the no-load losses were introduced in the model developed by Marques and Camacho [3] in order to a more realistic prediction of the total power loss and its breakdown through the different power loss sources. These results were obtained considering an oil volume of 1 litre. Generally the predictions are an accurate estimation of the experimental results, showing a slight difference on MINR and PAGD, as it can be seen from figures 7.1 and 7.7. As shown in Chapter 5, the churning losses present a higher loss source for PAGD and even with the consideration of the total power loss, it is an effect that couldn't be neglected as shown in figure 7.8. Churning losses are one of the most important component for PAGD, which may indicate a strong correlation between this phenomenon and oil density, since this is the oil that presents the highest density. In a previous work Changenet *et al.* [45] found that oil aeration plays an important role in gear churning losses. Aeration is related to the oil chemical properties, namely oil surface tension which dictates the amount and diameter of air bubbles that are formed in the oil sump. In the present work it was not possible to measure the surface tension of the different oils, however PAGD's surface tension should be quite different of the other lubricants as it was experimentally observed in the interactions between this oil and the different surfaces compared to the other lubricants. This may contribute to explain some of the differences that were observed. The total power loss in the planetary gearbox is given by equation (7.1).

$$P_V = P_{VZ0} + P_{VZP} + P_{VL} + P_{VD} + P_{VX} \tag{7.1}$$

Where the total power loss in bearings is calculated with equation (7.2).

$$P_{VL} = P_{VL}^{FCNRB} + P_{VL}^{TRB} + P_{VL}^{DGBB} \tag{7.2}$$

## 7.1 MINR

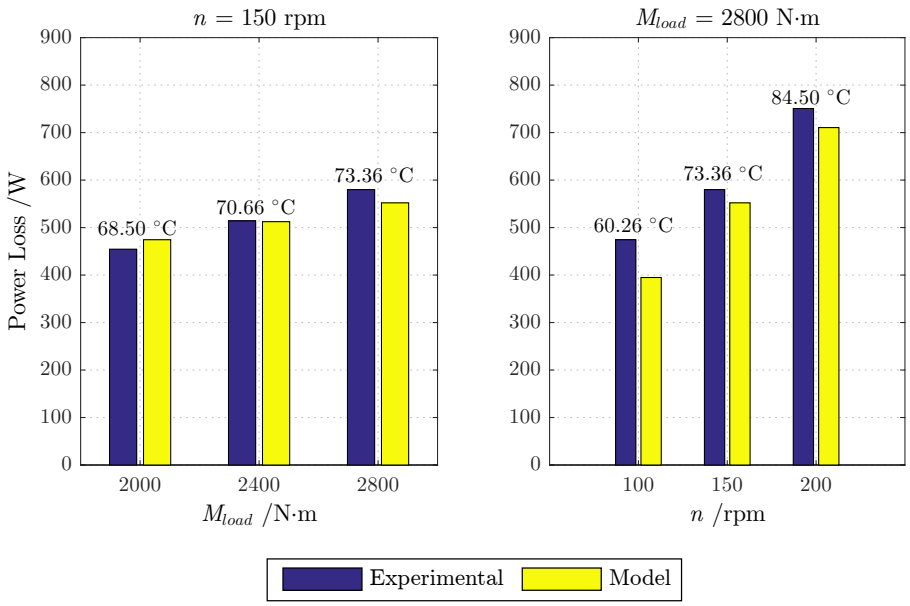


Figure 7.1: Experimental *vs.* numerical power loss for MINR.

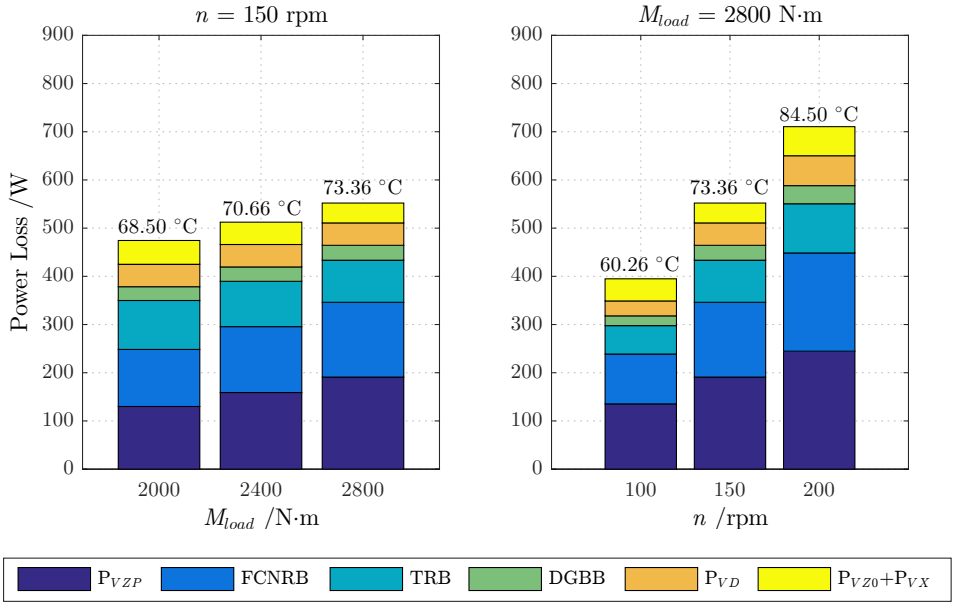


Figure 7.2: Global power loss (numerical) for MINR divided in its different components.

## 7.2 PAOR

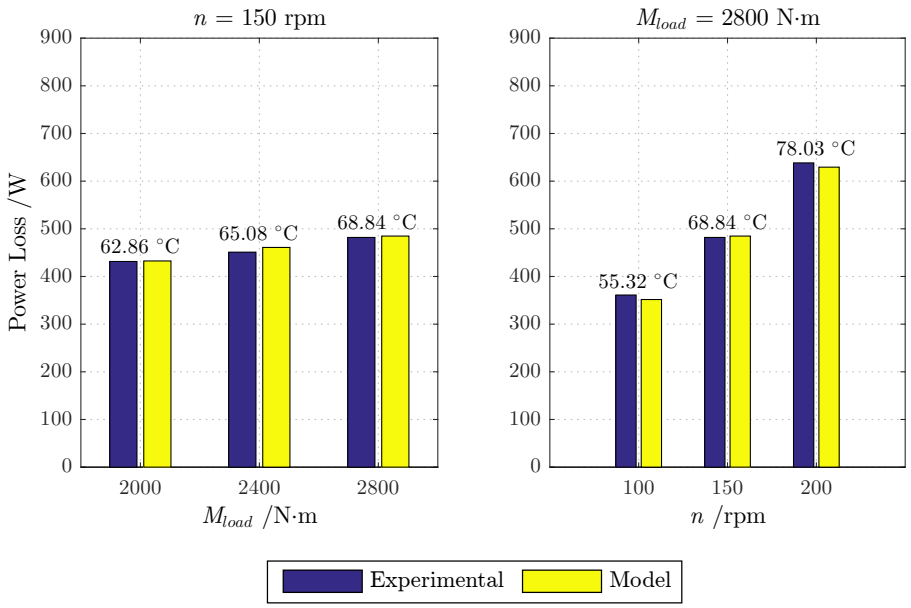


Figure 7.3: Experimental *vs.* numerical power loss for PAOR.

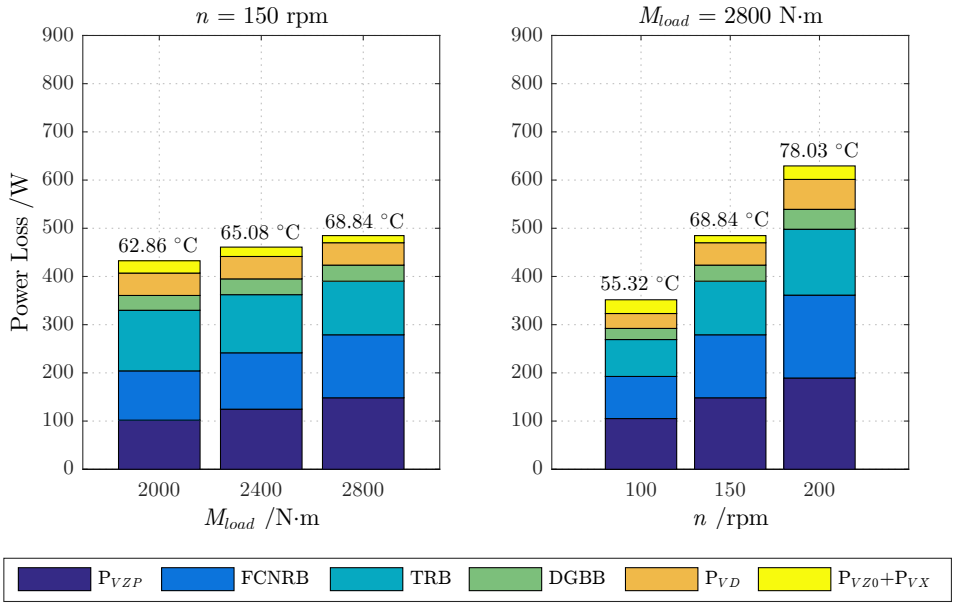


Figure 7.4: Global power loss (numerical) for PAOR divided in its different components.

## 7.3 MINE

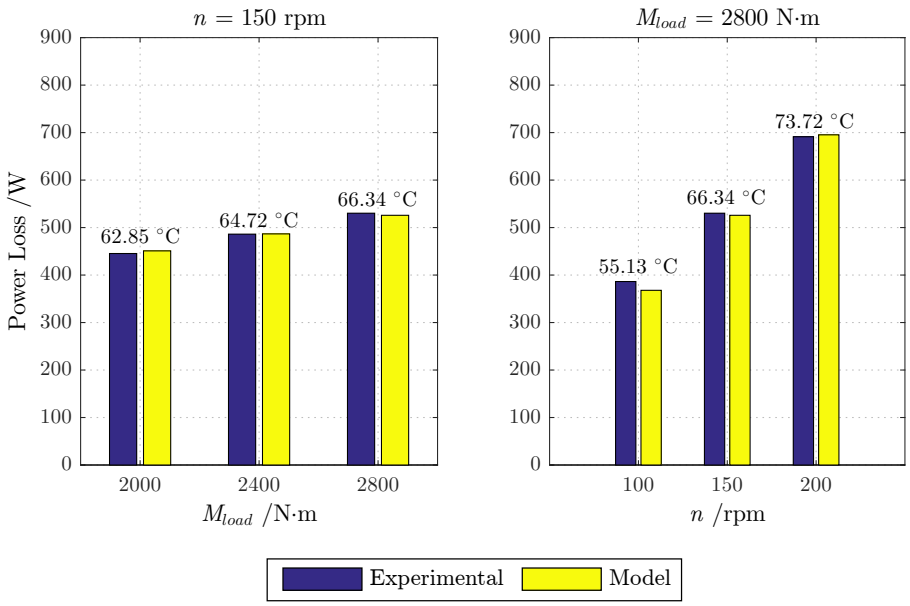


Figure 7.5: Experimental *vs.* numerical power loss for MINE.

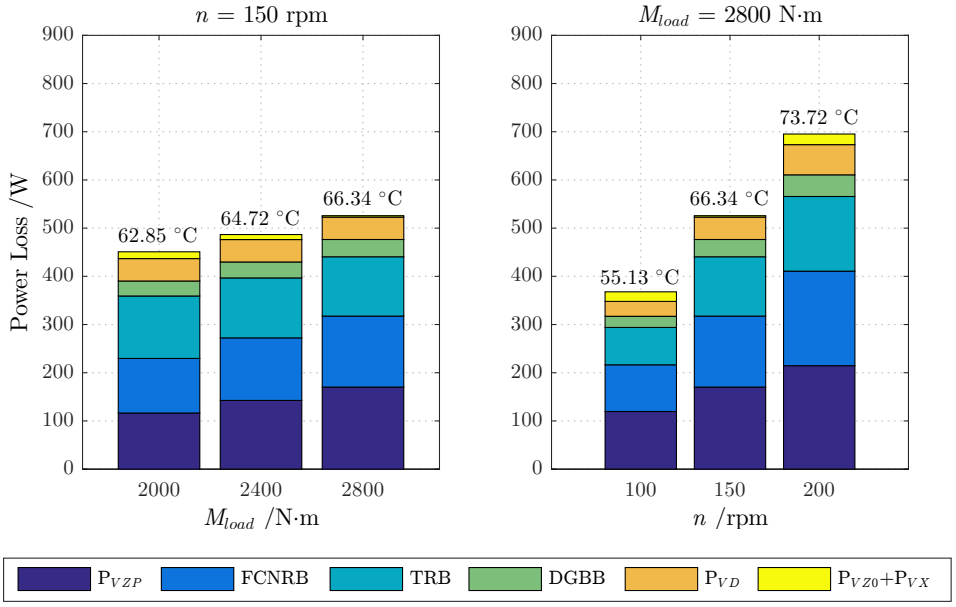


Figure 7.6: Global power loss (numerical) for MINE divided in its different components.

## 7.4 PAGD

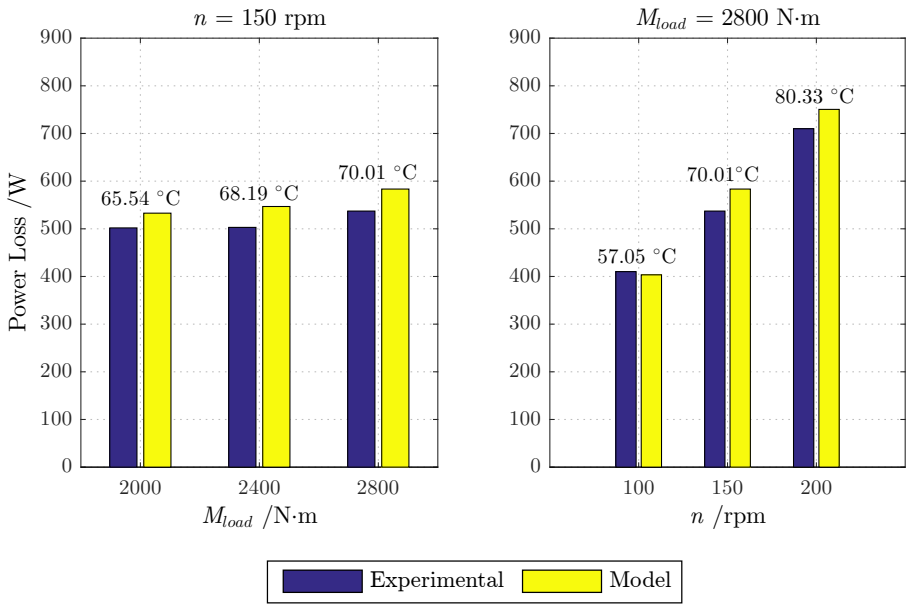


Figure 7.7: Experimental *vs.* numerical power loss for PAGD.

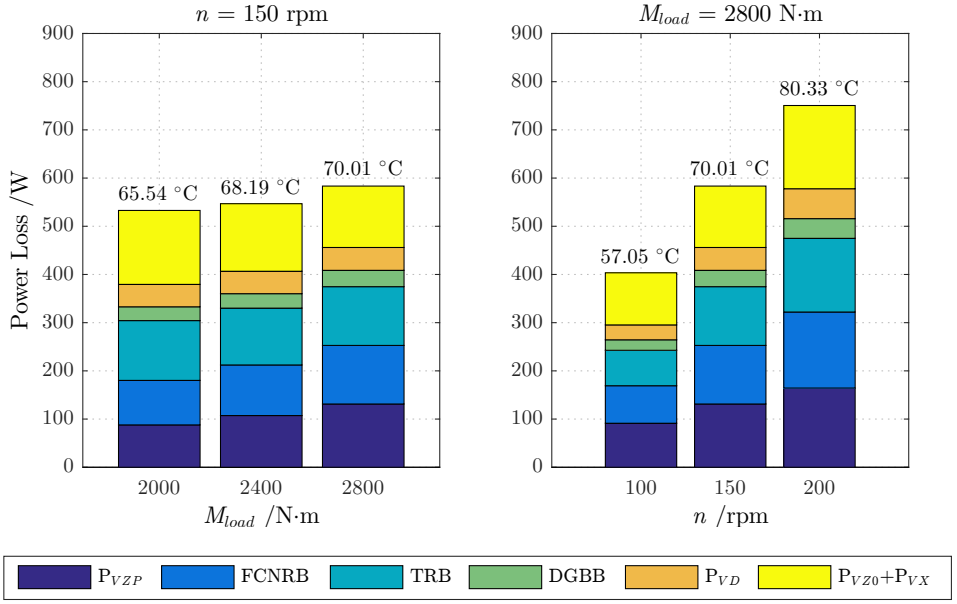


Figure 7.8: Global power loss (numerical) for PAGD divided in its different components.

## 7.5 Oils Comparison

The values of global power loss divided by each component are also presented under a tabular form in table 7.1.

Table 7.1: Global power loss divided in its different components for $M_{load}$ = 2800 N·m and $n$ = 150 rpm.

| | **Power Loss** /W | | | | **Power Loss** /% | | | |
|---|---|---|---|---|---|---|---|---|
| **Oil (1 L)** | MINR | PAOR | MINE | PAGD | MINR | PAOR | MINE | PAGD |
| $P_{VZP}$ | 191.00 | 148.30 | 170.30 | 131.30 | 34.59 | 30.59 | 32.38 | 22.51 |
| $P_{VL}^{FCNRB}$ | 155.20 | 130.70 | 147.30 | 121.50 | 28.11 | 26.96 | 28.01 | 20.83 |
| $P_{VL}^{TRB}$ | 87.35 | 111.20 | 123.10 | 121.90 | 15.82 | 22.94 | 23.41 | 20.89 |
| $P_{VL}^{DGBB}$ | 30.87 | 33.37 | 35.82 | 33.89 | 5.59 | 6.88 | 6.81 | 5.81 |
| $P_{VD}$ | 46.52 | 46.47 | 46.45 | 47.41 | 8.43 | 9.59 | 8.83 | 8.13 |
| $P_{VZ0}$+$P_{VX}$ | 41.19 | 14.73 | 2.96 | 127.40 | 7.46 | 3.04 | 0.56 | 21.84 |
| **Total** | 552.13 | 484.77 | 525.93 | 583.40 | 100 | 100 | 100 | 100 |

# CHAPTER 8

# Conclusions

At the end of this work it is possible to reach some important conclusions:

- Churning phenomenon involves a high number of variables and it is very complex to model.
- No-load torque losses decrease with the increase of rotation speed or load torque.
- MINE is the only oil that presents slightly higher value of no-load torque loss for a smaller volume.
- The results of no-load torque loss presented better consistency for constant speed than for constant load torque.
- PAGD was the only oil which showed significant differences for the two oil volumes used. The other lubricants proved to be quite indifferent to the different volumes.
- Tapered roller bearings are the major source of power loss. The component that provides the lowest power loss source are shaft seals.
- For churning power loss, all the oils showed the same behavior in the continuous tests.
- The no-load losses represent almost half of the total power loss in the planetary gearbox.
- PAGD has the highest overall power loss.

# CHAPTER 9

# Future Works

As it was seen, the no-load torque results allowed to improve a model to predict the total power loss in a planetary gearbox. However, the churning phenomenon still presents serious challenges.

The following works are suggested:

- Repeat the no-load torque measurements with deep groove ball bearings instead of tapered roller bearings and see the effect on the total power loss.
- Repeat the no-load torque measurements with different oil volumes to try to understand the oil level influence.
- Do a dimensional analysis on the churning phenomenon and try to understand its dependence on the several variables involved.
- For the continuous tests, represent the variation of each one of the power loss sources.
- Through a CFD analysis try to understand if the shape of the planet carrier could be optimized to reduce the auxiliary power losses.

# Bibliography


[1] The Guardian. Portugal runs for four days straight on renewable energy alone. https://www.theguardian.com/environment/2016/may/18/portugal-runs-for-four-days-straight-on-renewable-energy-alone, 2016. Accessed: 20/06/2016.

[2] Carlos M.C.G. Fernandes, Pedro M.T. Marques, Ramiro C. Martins, and Jorge H.O. Seabra. Gearbox power loss. part iii: Application to a parallel axis and a planetary gearbox. *Tribology International*, 88:317 – 326, 2015.

[3] Pedro M.T. Marques, Raquel Camacho, Ramiro C. Martins, and Jorge H.O. Seabra. Efficiency of a planetary multiplier gearbox: Influence of operating conditions and gear oil formulation. *Tribology International*, 92(0):272 – 280, 2015.

[4] P. Luke and A. Olver. A study of churning losses in dip-lubricated spur gears. *Journal of Instituition of Mechanical Engineers*, 213(Part G), 1999.

[5] EWEA European Wind Energy Association. Wind energy 2015 european statistics. http://www.ewea.org/fileadmin/files/library/publications/statistics/EWEA-Annual-Statistics-2015.pdf, 2015. Accessed: 19/04/2016.

[6] Global Wind Energy Council. Global cumulative installed capacity 2000-2015. http://www.gwec.net/global-figures/graphs/, 2015. Accessed: 26/04/2016.

[7] Carlos M.C.G. Fernandes, Luis Blazquez, Jorge Sanesteban, Ramiro C. Martins, and Jorge H.O. Seabra. Energy efficiency tests in a full scale wind turbine gearbox. *Tribology International*, 101:375 – 382, 2016.

[8] Carlos M.C.G. Fernandes, Maroua Hammami, Ramiro C. Martins, and Jorge H.O. Seabra. Power loss prediction: Application to a 2.5 MW wind turbine gearbox. *Institution of Mechanical Engineers*, 0(0):1 – 13, 2015.

[9] M.B. Peterson, W.O. Winer, and American Society of Mechanical Engineers. Research Committee on Lubrication. *Wear Control Handbook*. ASME centennial research project. American Society of Mechanical Engineers, 1980.

[10] Mobil Industrial Lubricants. Wind turbine trasmission system. http://www.mobilindustrial.com/ind/english/yourindustry_energy_wind_schematics.aspx#/. Accessed: 21/04/2016.

[11] Carlos M.C.G. Fernandes, Pedro M.T. Marques, Ramiro C. Martins, and Jorge H.O. Seabra. Gearbox power loss. part i: Losses in rolling bearings. *Tribology International*, 88:298 – 308, 2015.

[12] Carlos M.C.G. Fernandes, Pedro M.T. Marques, Ramiro C. Martins, and Jorge H.O. Seabra. Gearbox power loss. part ii: Friction losses in gears. *Tribology International*, 88:309 – 316, 2015.

[13] D. Pereira. Torque loss in a planetary multiplier gearbox: Influence of operating conditions and gear oil formulation. Master's thesis, Faculdade de Engenharia da Universidade do Porto, 2013.

[14] R. Camacho. Torque loss in a planetary multiplier gearbox: Influence of operating conditions and gear oil formulation. Master's thesis, Faculdade de Engenharia da Universidade do Porto, 2014.

[15] Von Kármán. On laminar and turbulent friction. *Zeitschrift für angewandte mathematik und mechanik*, 1(4), 1921.

[16] J. W. Daily and R.E. Neece. Chamber dimensions effect on induced flow and frictional resistance of enclosed rotating disks. *Journal of Basic Engineering*, 82(1):217–232, 1960.

[17] R. W. Mann and C.H. Marston. Friction drag on bladed disks in housings. *Journal of Basic Engineering*, 83(4):719–723, 1961.

[18] R. J. Boness. Churning losses of discs and gears running partially submerged in oil. *Procedings of ASME International Power Transmission Gearing Conference*, 1:355–359, 1989.

[19] A. S. Terekhov. Basic problem of heat calculation of gear reducers. International Conference on Motion and Power Transmissions, pages 490–495. Proceeding of Japanese Society of Mechanichal Engeners, November 1991.

[20] B.-R. Höhn, K. Michaelis, and T. Vollmer. Thermal rating of gear drives: Balance between power loss and heat dissipation. *AGMA Technical Paper*, 1996.

[21] C. Changenet, G. Leprince, F. Ville, and P. Velex. A note on flow regimes and churning loss modeling. *Journal of Mechanical Design*, 133(12):121009, 2011.

[22] D. Talbot, A. Kahraman, and Seetharaman S. A helical gear pair pocketing power loss model. *Journal of Tribology*, 136, 2014.

[23] F Concli and C Gorla. Computational and experimental analysis of the churning power losses in an industrial planetary speed reducer. In *9th International Conference on Advances in Fluid Mechanics-Advances in Fluid Mechanics IX, WIT Transactions on Engineering Sciences*, volume 74, pages 287–298, 2012.

[24] Pedro M.T. Marques. Trabalho de Mecânica de Fluidos Computacional. 2013.

[25] B.-R. Höhn, K. Michaelis, and M. Hinterstoißer. Optimization of gearbox efficiency. *goriva i maziva*, 48(4):462–480, 2009.

[26] H. Ohlendorf. *Verlustleistung und Erwärmung von Stirnrädern.* PhD thesis, Dissertation TU München, 1958.

[27] G. Niemann and H. Winter. *Maschinenelemente: Band 2: Getriebe allgemein, Zahnradgetriebe - Grundlagen, Stirnradgetriebe.* Maschinenelemente /Gustav Niemann. Springer, 1989.

[28] E. Buckingham. *Analytical mechanics of gears.* Dover Books for Engineers. McGraw-Hill Book Co., 1949.

[29] B. Kelley and A. Lemanski. Lubrication of involute gearing. *Conference on Lubrication and Wear,Proceedings of the Institution of Mechanical Engineers*, 182:173–184, 1967.

[30] K. Michaelis and B. R. Höhn. Influence of lubricants on power loss of cylindrical gears. *S T L E Tribology Transactions*, 37(1):161–167, 1994.

[31] L. Schlenk. *Unterscuchungen zur Fresstragfähigkeit von Grozahnrädern.* PhD thesis, Dissertation TU München, 1994.

[32] Carlos M.C.G. Fernandes, Ramiro C. Martins, and Jorge H.O. Seabra. Torque loss of type C40 FZG gears lubricated with wind turbine gear oils. *Tribology International*, (0):–, 2013.

[33] ISO 6336-4. Calculation of load capacity of spur and helical gears-Part 4. *ISO*, 1998.

[34] A. Doleschel. Wirkungsgradtest, vergleichende beurteilung des einflusses von schmierstoffen auf den wirkungsgrad bei zahnradgetrieben. *FVAForschungsvorhaben Nr. 345, FVA Forschungsheft Nr. 664*, 2002.

[35] Xu Hai. *Development of a Generalized Mechanical Efficiency Prediction Methodology for Gear Pairs.* PhD thesis, The Ohio State University, 2005.

[36] SKF. *SKF General Catalogue 6000 EN.* SKF, 2013.

[37] SKF. *SKF Hauptkatalog Nr. 2800T.* SKF, 1981.

[38] Eschmann Hasbargen Weigand. *Ball and Roller Bearings - Theory, Design, and Application.* Wiley, 1985.

[39] T.A. Harris and M.N. Kotzalas. *Essential Concepts of Bearing Technology, Fifth Edition.* Rolling Bearing Analysis, Fifth Edtion. CRC Press, 2006.

[40] T.A. Harris and M.N. Kotzalas. *Advanced Concepts of Bearing Technology,: Rolling Bearing Analysis, Fifth Edition.* Rolling Bearing Analysis, Fifth Edtion. CRC Press, 2006.

[41] Freudenberg Simrit GmbH & Co. KG. *Technische Grundlagen, Simerringue und Rotationsdichtungen.* Freudenberg Simrit GmbH & Co. KG, Technisches Handbuch 2007.

[42] H. Linke. Stirnradverzahnung. *Hanser Verlag*, 1996.

[43] J. Kettler. *Ölsumpftemperatur von Planetengetrieben: Abschlußbericht ; Forschungsvorhaben Nr. 313: Planetengetriebe-Sumpftemperatur.* Forschungsheft: Forschungsvereinigung Antriebstechnik. FVA, 2002.

[44] KLUBER Lubrication. Special lubricants for wind turbines. `http://www.klueber.com/ecomaXL/files/B16_PAW_wind_UK_080807_v01_04[1].pdf`, 2011. Accessed: 12/05/2016.

[45] C. Changenet and P. Velex. A model for the prediction of churning losses in geared transmissions—preliminary results. *Journal of Mechanical Design*, 129(1):128–133, 2007.

# Appendices

# APPENDIX A

## Planetary Gearbox Specifications

# SP+ 240 MF 1/2-stage

| | | | | | 1-stage | | | | | 2-stage | | | | | | | | |
|---|---|---|---|---|---|---|---|---|---|---|---|---|---|---|---|---|---|---|
| **Ratio** [a] | | | ***i*** | | **3** | **4** | **5** | **7** | **10** | **16** | **20** | **25** | **28** | **35** | **40** | **50** | **70** | **100** |
| cymex®-optimized acceleration torque (please contact us regarding the design) | | | $T_{2Bcym}$ | Nm | - Please contact us - | | | | | | | | | | | | | |
| | | | | in.lb | | | | | | | | | | | | | | |
| Max. acceleration torque (max. 1000 cycles per hour) | | | $T_{2B}$ | Nm | 2750 | 4500 | 4500 | 4300 | 3400 | 4500 | 4500 | 4500 | 4500 | 4500 | 4000 | 4300 | 4300 | 3400 |
| | | | | in.lb | 24338 | 39825 | 39825 | 38055 | 30090 | 39825 | 39825 | 39825 | 39825 | 39825 | 35400 | 38055 | 38055 | 30090 |
| Nominal output torque (with $n_{1N}$) | | | $T_{2N}$ | Nm | 1500 | 2500 | 2500 | 2300 | 1700 | 2500 | 2500 | 2500 | 2500 | 2500 | 2500 | 2500 | 2300 | 1700 |
| | | | | in.lb | 13275 | 22125 | 22125 | 20355 | 15045 | 22125 | 22125 | 22125 | 22125 | 22125 | 22125 | 22125 | 20355 | 15045 |
| Emergency stop torque (permitted 1000 times during the service life of the gearhead) | | | $T_{2Not}$ | Nm | 6800 | 8500 | 8500 | 8500 | 6800 | 8500 | 8500 | 8500 | 8500 | 8500 | 8500 | 8500 | 8500 | 6800 |
| | | | | in.lb | 60180 | 75225 | 75225 | 75225 | 60180 | 75225 | 75225 | 75225 | 75225 | 75225 | 75225 | 75225 | 75225 | 60180 |
| Nominal input speed (with $T_{2N}$ and 20°C ambient temperature) [b] | | | $n_{1N}$ | rpm | 1000 | 1000 | 1200 | 1500 | 1700 | 2300 | 2500 | 2500 | 2500 | 2500 | 2500 | 2500 | 2800 | 2800 |
| Max. input speed | | | $n_{1Max}$ | rpm | 2500 | 2500 | 2500 | 2500 | 2500 | 3500 | 3500 | 3500 | 3500 | 3500 | 3500 | 3500 | 3500 | 3500 |
| Mean no load running torque (with $n_1$ = 2000 rpm and 20°C gearhead temperature) | | | $T_{012}$ | Nm | 45 | 35 | 26 | 16 | 11 | 11 | 9,0 | 8,0 | 7,0 | 6,0 | 5,0 | 4,5 | 4,0 | 4,0 |
| | | | | in.lb | 398 | 310 | 230 | 142 | 97 | 97 | 80 | 71 | 62 | 53 | 44 | 40 | 35 | 35 |
| Max. torsional backlash | | | $j_t$ | arcmin | Standard ≤ 3 / Reduced ≤ 1 | | | | | Standard ≤ 5 / Reduced ≤ 3 | | | | | | | | |
| Torsional rigidity | | | $C_{t21}$ | Nm/ arcmin | 550 | | | | | 550 | | | | | | | | |
| | | | | in lb/ arcmin | 4868 | | | | | 4868 | | | | | | | | |
| Max. axial force [c] | | | $F_{2AMax}$ | N | 33000 | | | | | 33000 | | | | | | | | |
| | | | | $lb_f$ | 7425 | | | | | 7425 | | | | | | | | |
| Max. radial force [c] | | | $F_{2RMax}$ | N | 30000 | | | | | 30000 | | | | | | | | |
| | | | | $lb_f$ | 6750 | | | | | 6750 | | | | | | | | |
| Max. tilting moment | | | $M_{2KMax}$ | Nm | 5000 | | | | | 5000 | | | | | | | | |
| | | | | in.lb | 44250 | | | | | 44250 | | | | | | | | |
| Efficiency at full load | | | η | % | 97 | | | | | 94 | | | | | | | | |
| Service life (For calculation, see the Chapter "Information") | | | $L_h$ | h | > 20000 | | | | | > 20000 | | | | | | | | |
| Weight incl. standard adapter plate | | | $m$ | kg | 77 | | | | | 76 | | | | | | | | |
| | | | | $lb_m$ | 170 | | | | | 168 | | | | | | | | |
| Operating noise (with $i$=10 and $n_1$ = 3000 rpm no load) | | | $L_{PA}$ | dB(A) | ≤ 66 | | | | | | | | | | | | | |
| Max. permitted housing temperature | | | | °C | +90 | | | | | | | | | | | | | |
| | | | | F | 194 | | | | | | | | | | | | | |
| Ambient temperature | | | | °C | -15 to +40 | | | | | | | | | | | | | |
| | | | | F | 5 to 104 | | | | | | | | | | | | | |
| Lubrication | | | | | Lubricated for life | | | | | | | | | | | | | |
| Paint | | | | | Blue RAL 5002 | | | | | | | | | | | | | |
| Direction of rotation | | | | | Motor and gearhead same direction | | | | | | | | | | | | | |
| Protection class | | | | | IP 65 | | | | | | | | | | | | | |
| Moment of inertia (relates to the drive) | M | 48 | $J_1$ | $kgcm^2$ | - | - | - | - | - | 39.2 | 34.6 | 33.2 | 30.5 | 29.7 | 28.2 | 27.9 | 27.6 | 27.5 |
| | | | | $10^{-3}$ in lb $s^2$ | | | | | | 34.7 | 30.6 | 29.4 | 27.0 | 26.3 | 25.0 | 24.7 | 24.4 | 24.3 |
| Clamping hub diameter [mm] | O | 60 | $J_1$ | $kgcm^2$ | 260.2 | 198.2 | 163.0 | 84.4 | 70.8 | - | - | - | - | - | - | - | - | - |
| | | | | $10^{-3}$ in lb $s^2$ | 230.3 | 175.4 | 144.3 | 74.7 | 62.7 | | | | | | | | | |

Reduced mass moments of inertia available on request.

[a] Other ratios available on request
[b] For higher ambient temperatures, please contact us
[c] Refers to center of the output shaft or flange

# APPENDIX B

# No-Load Torque Loss Measurements

## B.1 MINR

### B.1.1 1 L

Table B.1: No-load torque loss measurements for MINR (S1).

| Oil: | MINR | | | | | |
|---|---|---|---|---|---|---|
| Test Number: | 1 | | | 2 | | |
| | $M_{load}$ /N·m | | | | | |
| $n$ /rpm | 2000 | 2400 | 2800 | 2000 | 2400 | 2800 |
| 100 | - | - | 13.60 | - | - | 14.24 |
| 150 | 13.44 | 12.68 | 11.76 | 14.16 | 13.44 | 12.60 |
| 200 | - | - | 11.00 | - | - | 11.44 |

Table B.2: No-load torque loss measurements for MINR (S2).

| Oil: | MINR | | | | | |
|---|---|---|---|---|---|---|
| Test Number: | 3 | | | 4 | | |
| | $M_{load}$ /N·m | | | | | |
| $n$ /rpm | 2000 | 2400 | 2800 | 2000 | 2400 | 2800 |
| 100 | - | - | 14.12 | - | - | 14.16 |
| 150 | 13.60 | 12.80 | 11.96 | 13.84 | 13.04 | 12.28 |
| 200 | - | - | 11.80 | - | - | 11.96 |

### B.1.2 0.75 L

Table B.3: No-load torque loss measurements for MINR (S1).

| Oil: | MINR | | | | | |
|---|---|---|---|---|---|---|
| Test Number: | 5 | | | 6 | | |
| | $M_{load}$ /N·m | | | | | |
| $n$ /rpm | 2000 | 2400 | 2800 | 2000 | 2400 | 2800 |
| 100 | - | - | 13.48 | - | - | 13.44 |
| 150 | 13.88 | 13.24 | 12.40 | 13.60 | 12.96 | 12.00 |
| 200 | - | - | 11.48 | - | - | 11.20 |

Table B.4: No-load torque loss measurements for MINR (S2).

| Oil: | MINR | | | | | |
|---|---|---|---|---|---|---|
| Test Number: | 7 | | | 8 | | |
| | $M_{load}$ /N·m | | | | | |
| $n$ /rpm | 2000 | 2400 | 2800 | 2000 | 2400 | 2800 |
| 100 | - | - | 14.44 | - | - | 14.48 |
| 150 | 13.32 | 12.76 | 11.80 | 13.84 | 13.24 | 12.32 |
| 200 | - | - | 11.72 | - | - | 12.08 |

## B.2 PAOR

### B.2.1 1 L

Table B.5: No-load torque loss measurements for PAOR (S1).

| Oil: | PAOR | | | | | |
|---|---|---|---|---|---|---|
| Test Number: | 9 | | | 10 | | |
| | $M_{load}$ /N·m | | | | | |
| $n$ /rpm | 2000 | 2400 | 2800 | 2000 | 2400 | 2800 |
| 100 | - | - | 13.80 | - | - | 14.28 |
| 150 | 14.04 | 13.20 | 12.12 | 14.36 | 13.56 | 12.36 |
| 200 | - | - | 11.52 | - | - | 11.72 |

Table B.6: No-load torque loss measurements for PAOR (S2).

| Oil: | PAOR | | | | | |
|---|---|---|---|---|---|---|
| Test Number: | 11 | | | 12 | | |
| | $M_{load}$ /N·m | | | | | |
| $n$ /rpm | 2000 | 2400 | 2800 | 2000 | 2400 | 2800 |
| 100 | - | - | 14.80 | - | - | 14.84 |
| 150 | 14.00 | 13.32 | 12.36 | 14.12 | 13.32 | 12.52 |
| 200 | - | - | 12.48 | - | - | 12.52 |

### B.2.2 0.75 L

Table B.7: No-load torque loss measurements for PAOR (S1).

| Oil: | PAOR | | | | | |
|---|---|---|---|---|---|---|
| Test Number: | 13 | | | 14 | | |
| | $M_{load}$ /N·m | | | | | |
| $n$ /rpm | 2000 | 2400 | 2800 | 2000 | 2400 | 2800 |
| 100 | - | - | 12.76 | - | - | 13.44 |
| 150 | 13.52 | 12.88 | 11.80 | 14.16 | 13.36 | 12.20 |
| 200 | - | - | 11.72 | - | - | 11.80 |

Table B.8: No-load torque loss measurements for PAOR (S2).

| Oil: | PAOR | | | | | |
|---|---|---|---|---|---|---|
| Test Number: | 15 | | | 16 | | |
| | $M_{load}$ /N·m | | | | | |
| $n$ /rpm | 2000 | 2400 | 2800 | 2000 | 2400 | 2800 |
| 100 | - | - | 14.16 | - | - | 14.40 |
| 150 | 13.92 | 13.04 | 12.12 | 14.00 | 13.36 | 12.04 |
| 200 | - | - | 12.20 | - | - | 11.84 |

## B.3 MINE

### B.3.1 1 L

Table B.9: No-load torque loss measurements for MINE (S1).

| Oil: | MINE | | | | | |
|---|---|---|---|---|---|---|
| Test Number: | 17 | | | 18 | | |
| | $M_{load}$ /N·m | | | | | |
| $n$ /rpm | 2000 | 2400 | 2800 | 2000 | 2400 | 2800 |
| 100 | - | - | 13.08 | - | - | 13.36 |
| 150 | 13.56 | 12.76 | 12.24 | 13.92 | 13.20 | 12.68 |
| 200 | - | - | 12.32 | - | - | 12.56 |

Table B.10: No-load torque loss measurements for MINE (S2).

| Oil: | MINE | | | | | |
|---|---|---|---|---|---|---|
| Test Number: | 19 | | | 20 | | |
| | $M_{load}$ /N·m | | | | | |
| $n$ /rpm | 2000 | 2400 | 2800 | 2000 | 2400 | 2800 |
| 100 | - | - | 13.76 | - | - | 14.68 |
| 150 | 13.52 | 13.08 | 12.56 | 13.76 | 13.24 | 12.64 |
| 200 | - | - | 13.04 | - | - | 13.12 |

### B.3.2 0.75 L

Table B.11: No-load torque loss measurements for MINE (S1).

| Oil: | MINE | | | | | |
|---|---|---|---|---|---|---|
| Test Number: | 21 | | | 22 | | |
| | $M_{load}$ /N·m | | | | | |
| $n$ /rpm | 2000 | 2400 | 2800 | 2000 | 2400 | 2800 |
| 100 | - | - | 13.96 | - | - | 13.64 |
| 150 | 13.08 | 13.40 | 12.84 | 14.00 | 13.32 | 12.92 |
| 200 | - | - | 13.04 | - | - | 13.00 |

Table B.12: No-load torque loss measurements for MINE (S2).

| Oil: | MINE | | | | | |
|---|---|---|---|---|---|---|
| Test Number: | 23 | | | 24 | | |
| | $M_{load}$ /N·m | | | | | |
| $n$ /rpm | 2000 | 2400 | 2800 | 2000 | 2400 | 2800 |
| 100 | - | - | 15.60 | - | - | 15.60 |
| 150 | 14.24 | 13.60 | 12.92 | 13.68 | 13.08 | 12.64 |
| 200 | - | - | 13.84 | - | - | 13.24 |

## B.4 PAGD

### B.4.1 1 L

Table B.13: No-load torque loss measurements for PAGD (S1).

| Oil: | PAGD | | | | | |
|---|---|---|---|---|---|---|
| Test Number: | 25 | | | 26 | | |
| | $M_{load}$ /N·m | | | | | |
| $n$ /rpm | 2000 | 2400 | 2800 | 2000 | 2400 | 2800 |
| 100 | - | - | 21.04 | - | - | 21.00 |
| 150 | 21.92 | 20.64 | 19.92 | 21.88 | 20.76 | 20.00 |
| 200 | - | - | 19.72 | - | - | 19.72 |

Table B.14: No-load torque loss measurements for PAGD (S2).

| Oil: | PAGD | | | | | |
|---|---|---|---|---|---|---|
| Test Number: | 27 | | | 28 | | |
| | $M_{load}$ /N·m | | | | | |
| $n$ /rpm | 2000 | 2400 | 2800 | 2000 | 2400 | 2800 |
| 100 | - | - | 22.28 | - | - | 22.48 |
| 150 | 22.24 | 20.72 | 19.92 | 22.56 | 21.20 | 20.20 |
| 200 | - | - | 20.00 | - | - | 20.20 |

### B.4.2 0.75 L

Table B.15: No-load torque loss measurements for PAGD (S1).

| Oil: | PAGD | | | | | |
|---|---|---|---|---|---|---|
| Test Number: | 29 | | | 30 | | |
| | $M_{load}$ /N·m | | | | | |
| $n$ /rpm | 2000 | 2400 | 2800 | 2000 | 2400 | 2800 |
| 100 | - | - | 18.68 | - | - | 18.64 |
| 150 | 19.64 | 18.60 | 18.08 | 19.92 | 18.88 | 18.28 |
| 200 | - | - | 18.32 | - | - | 18.32 |

Table B.16: No-load torque loss measurements for PAGD (S2).

| Oil: | PAGD | | | | | |
|---|---|---|---|---|---|---|
| Test Number: | 31 | | | 32 | | |
| | $M_{load}$ /N·m | | | | | |
| $n$ /rpm | 2000 | 2400 | 2800 | 2000 | 2400 | 2800 |
| 100 | - | - | 19.64 | - | - | 19.76 |
| 150 | 19.68 | 18.60 | 17.92 | 19.80 | 18.60 | 17.88 |
| 200 | - | - | 17.40 | - | - | 17.60 |